© 2021. Published by The Company of Biologists Ltd | Development (2021) 148, dev199460. doi:10.1242/dev.199460

RESEARCH ARTICLE

Defective mesothelium and limited physical space are drivers of dysregulated lung development in a genetic model of congenital diaphragmatic hernia

Rachel M. Gilbert[1], Laurel E. Schappell[1] and Jason P. Gleghorn[1,2,*]

ABSTRACT

Congenital diaphragmatic hernia (CDH) is a developmental disorder associated with diaphragm defects and lung hypoplasia. The etiology of CDH is complex and its clinical presentation is variable. We investigated the role of the pulmonary mesothelium in dysregulated lung growth noted in the *Wt1* knockout mouse model of CDH. Loss of WT1 leads to intrafetal effusions, altered lung growth, and branching defects prior to normal closure of the diaphragm. We found significant differences in key genes; however, when *Wt1* null lungs were cultured *ex vivo*, growth and branching were indistinguishable from wild-type littermates. Micro-CT imaging of embryos *in situ* within the uterus revealed a near absence of space in the dorsal chest cavity, but no difference in total chest cavity volume in *Wt1* null embryos, indicating a redistribution of pleural space. The altered space and normal *ex vivo* growth suggest that physical constraints are contributing to the CDH lung phenotype observed in this mouse model. These studies emphasize the importance of examining the mesothelium and chest cavity as a whole, rather than focusing on single organs in isolation to understand early CDH etiology.

KEY WORDS: CDH, WT1, Branching morphogenesis, Diaphragm development, Micro-CT, Pleural cavity

INTRODUCTION

Congenital diaphragmatic hernia (CDH) is associated with severe morbidity and mortality and affects a large proportion of the population with an incidence rate of 1 in 3000 live births worldwide (Kardon et al., 2017). CDH manifests during embryonic development with a hole in the diaphragm, through which abdominal organs herniate into the pleural cavity, often resulting in unilateral pulmonary hypoplasia. A persistent challenge for treatment of CDH lies in the complex and varying clinical presentations and an unclear etiology of the congenital condition. CDH is not a monogenic disease and more than 100 different genes have been implicated in CDH (Donahoe et al., 2016; Holder et al., 2007; Yu et al., 2019). Moreover, only ∼30% of CDH cases can be associated with genetic abnormalities, which span a variety of different genetic pathways (Russell et al., 2012; Yu et al., 2019, 2015). In addition, although several studies have identified the pleuroperitoneal fold (PPF) cells as a cellular source of CDH, other cells or tissues likely also play a role in CDH etiology. Clearly, malformation of the diaphragm is a consequence of, and long thought to be the causative driver of CDH; however, evidence of changes in other organs, including the heart and lungs, has called this into question (Kardon et al., 2017). Of particular interest is the 'dual hit' hypothesis of CDH wherein there is an initial defect in the diaphragm and lung in early development (the first hit), which is subsequently exacerbated by organ herniation (the second hit). This hypothesis is supported by lung defects observed prior to normal closure of the diaphragm in small animal models (Keijzer et al., 2000; Merrell et al., 2015; Paris et al., 2015). These data, in combination with the variable expressivity and poor penetrance of genomic targets identified thus far, underscore the complexity in understanding CDH.

One gene that has been identified as a candidate in human and mouse models of CDH is Wilm's tumor -1 (*Wt1*). This gene has been found to be mutated in human cases of CDH, and when knocked out in mouse models, produces a CDH phenotype (Kardon et al., 2017; Yu et al., 2019). The WT1 knockout model of CDH produces both lung and diaphragmatic defects, but the lung defects have not been well characterized. WT1 is a transcription factor and is expressed by mesothelial cells of the pleural cavity. Importantly, the mesothelium is a tissue layer that covers the outer surface of the thoracic organs, including the heart, where it is called the epicardium, as well as the diaphragm and the lung (Hiriart et al., 2019). Whereas the roles of WT1 in the epicardium and diaphragmatic mesothelium have been more thoroughly examined, investigation into the role of WT1 in the lung mesothelium has been lacking. Whether WT1 is knocked out globally (Cano et al., 2013; Carmona et al., 2016; Kreidberg et al., 1993; Paris et al., 2015), or specifically in the PPFs of the diaphragmatic mesothelium (Carmona et al., 2016), WT1 loss causes diaphragmatic defects reminiscent of human CDH. However, in these studies, the effect to the lung was not examined beyond gross observations of pulmonary hypoplasia. Therefore, it is unclear whether this genetic model of CDH also supports the dual hit hypothesis of CDH.

Broadly speaking, comparatively little work has been done to understand the role of the lung mesothelium in morphogenesis, making this tissue much of a mystery during pulmonary development. Studies have demonstrated that during the pseudoglandular stage of development [embryonic day (E) 11.5-E16.5] the lung mesothelium expresses key genes, such as retinoic acid dehydrogenase (*Aldh1a2*) and fibroblast growth factor 9 (*Fgf9*), which are necessary for proper lung morphogenesis (Colvin et al., 1999; Malpel et al., 2000; Niederreither et al., 2002). Careful examination of the genes that have been positively linked to patient cases of CDH suggests that a defective mesothelium may be a driving factor in this condition. Retinoic acid is processed within the

[1]Departments of Biomedical Engineering, University of Delaware, Newark, DE 19716, USA. [2]Departments of Biological Sciences, University of Delaware, Newark, DE 19716, USA.

*Author for correspondence (gleghorn@udel.edu)

R.M.G., 0000-0003-2523-9483; L.E.S., 0000-0001-9215-2076; J.P.G., 0000-0003-1283-2966

Handling Editor: Patrick Tam
Received 31 January 2021; Accepted 14 April 2021

Development (2021) 148, dev199460. doi:10.1242/dev.199460

mesothelium from vitamin A via ALDH1a2, also referred to as RALDH2, and has been found to be defective in patients and mouse models of CDH (Baptista et al., 2005; Clugston et al., 2006; Coste et al., 2015; Greer et al., 2003; Kling and Schnitzer, 2007). Components of this pathway have also been found to be defective in isolated and familial human CDH cases, as well as teratogenic and genetic models of CDH (Clugston et al., 2006; Montedonico et al., 2008). However, to date, much of the focus in understanding CDH and the roles of the genes discussed have centered on the diaphragm and heart, with minimal attention to the lung mesothelium.

Given the strong data that support the dual hit hypothesis of CDH by demonstrated morphogenetic lung defects prior to normal diaphragmatic closure, we sought to characterize WT1 during lung development and examine the effect of *Wt1* knockout specifically as it relates to lung development. We show that WT1-expressing mesothelial cells are located along the dorsal lobes of the lung at the early pseudoglandular phase of growth. Upon global knockout of *Wt1*, a variety of gross morphological defects are present, including intrafetal effusion and airway branching abnormalities that deviated from typical lung branching morphology. These morphological defects were accompanied by changes in gene expression of key regulators of lung development. Importantly, all gene expression and branching defects were observed at E12.5, before normal closure of the diaphragm at E13.5, consistent with the dual hit hypothesis of lung and diaphragmatic defects prior to organ herniation (Keijzer et al., 2000). We found that atypical lung morphologies and altered growth existed throughout gestation in $Wt1^{-/-}$ mice; however, surprisingly, if the lungs were isolated and cultured *ex vivo*, the lung displayed growth rates and branching indistinguishable from those of wild-type and heterozygous lung explants. When gene expression was assayed after culture, we determined that these key genes were still significantly decreased, indicating that WT1 likely acts upstream of their expression. Upon examination of the whole embryo *in situ* using micro-CT, we observed decreased space available for the developing lung within the thorax, prior to organ herniation and diaphragmatic closure, suggesting that physical constraints of the chest cavity could be contributing to the initial CDH phenotype and morphological defects observed in this mouse model. The altered chest cavity environment at this early stage of development may play an unappreciated role in CDH etiology. These data highlight the need to understand both the genetic and mechanical regulators of lung development and CDH etiology. From these studies and the variable clinical severity seen in CDH patients, we conclude that when examining the early driving mechanisms of CDH, the condition needs to be considered in the context of the entire thoracic cavity, rather than in the context of individual organ dysfunction.

RESULTS

WT1 is absent along the trachea and main bronchi during pseudoglandular lung development

We investigated the role of WT1 in the lung mesothelium by first examining its expression pattern during normal development using whole-mount immunofluorescence and confocal microscopy. From E11 to E11.5, WT1 is ubiquitously present throughout the entire mesothelium covering the pulmonary lobes. However, on the trachea, WT1-positive cells were only present on the ventral surface, with a portion of expression lost near the ventral carina and no expression on the dorsal surface of the trachea (Fig. 1A,B). The esophagus lies on the dorsal surface of the trachea, so to ensure that this observed pattern was not a result of removing the esophagus during lung isolation, we examined lung explants with the esophagus still attached (Fig. 1C). Immunostaining validated an absence of WT1 positive mesothelial cells along the dorsal surface of the trachea and entirety of the esophagus.

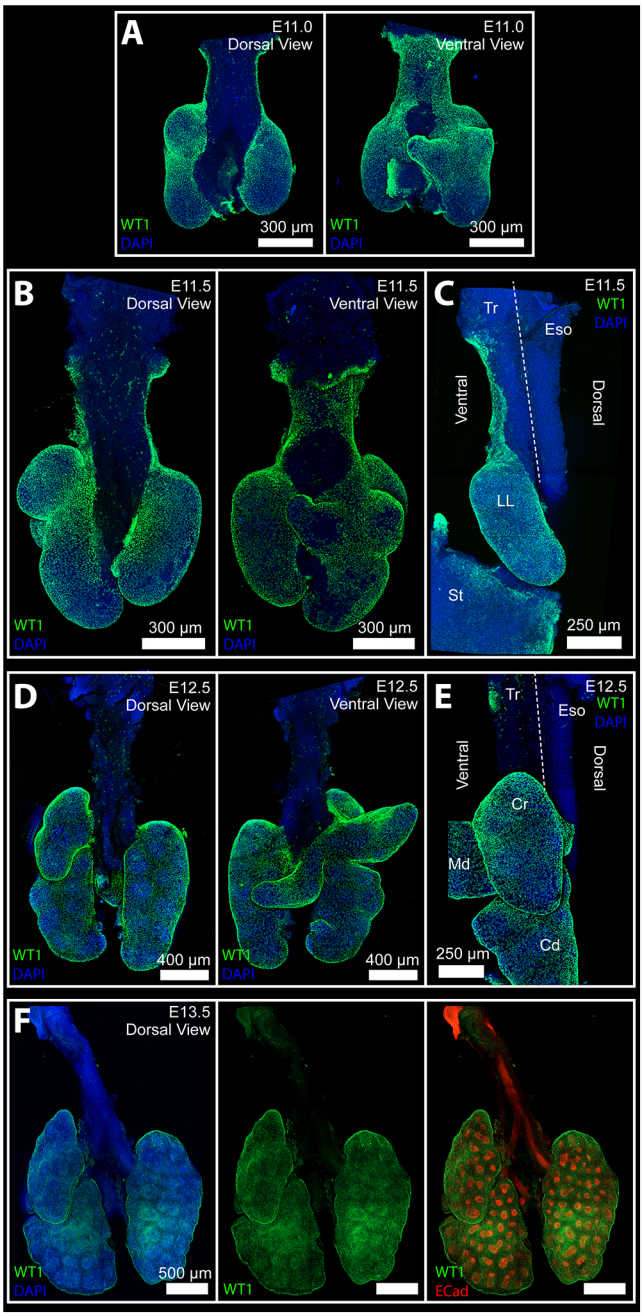

Fig. 1. The pattern of WT1 in the lung mesothelium changes throughout lung development. Lung explants were immunostained for WT1 (green) and co-stained with DAPI (blue) to visualize cell localization. (A) Dorsal and ventral view of a representative E11.0 lung explant. (B) Representative E11.5 lung explant. (C) Lateral view of a representative E11.5 lung explant with the esophagus (Eso) still attached to the dorsal surface of the trachea (Tr), with left lung (LL) and stomach (St) visible. (D) Dorsal and ventral view of a representative E12.5 lung explant. (E) Lateral view of a representative E12.5 lung explant with the esophagus still attached; cranial (Cr), middle (Md) and caudal (Cd) lung lobes are visible on the right lung. (F) Representative E13.5 lung explant with E-cadherin immunostaining (red) to label epithelial airways. All images shown are maximum projections of confocal *z*-stack images.

By E12.5, all WT1-positive cells were lost from both surfaces of the carina and upper regions of the left and right mainstem bronchi

Development (2021) 148, dev199460. doi:10.1242/dev.199460

(Fig. 1D,E) and remained absent in these regions for the duration of development. WT1-positive cells were present throughout the mesothelium covering the lung lobes and this pattern persisted through E13.5 (Fig. 1F). This pattern of WT1 expression suggested that changes in WT1 would likely affect the actively branching distal regions of the lung, rather than the trachea, during the pseudoglandular phase.

Knockout of WT1 induces gross anatomical and epithelial branching architecture changes

Past studies have performed global knockout of *Wt1* to investigate other organ compartments, such as the kidney (Kreidberg et al., 1993) and diaphragm (Carmona et al., 2016; Dingemann et al., 2011; Paris et al., 2015), with only passing mention to the effect of this knockout on the lung. Given the proposed theory that the lung can have defective growth before organ herniation in CDH (Keijzer et al., 2000), and the connection of *Wt1* knockout and CDH phenotype in mice (Kardon et al., 2017), we investigated how WT1 influences lung development. It is difficult to perform a lung mesothelial tissue-specific knockout of *Wt1* owing to the parallels in gene expression between the mesothelium of the lung, heart and diaphragm. To our knowledge, no gene has been identified as a lung mesothelial-specific gene that would allow for the generation of lung mesothelial-specific knockout of *Wt1*. Therefore, we performed a global knockout of *Wt1* and examined the specific effects on the lung.

Upon gross examination, *Wt1* null embryos presented with obvious intrafetal fluid effusion, predominantly in the upper body cavity, that was not present in heterozygous or wild-type embryos (Fig. 2A,C,E). We describe this fluid as intrafetal as the diaphragm has not completely developed at the early gestational ages examined and $Wt1^{-/-}$ embryos have known defects in the formation of pleuropericardial membranes (Norden et al., 2012), making precise description of the effusion type difficult to determine. However, grossly, almost all effusion fluid was located in the upper body cavity with obvious outward ventral and lateral displacement of the chest wall. These previously noted (Kreidberg et al., 1993) but otherwise uncharacterized effusions varied in severity but were consistently present in E12.5 embryos (Fig. 2C,E). The effusion fluid often contained blood that was visible, moved fluidly, and pooled in the lowest part of the body cavity, indicating that it was not clotted (Fig. 2E). Lungs explanted from $Wt1^{-/-}$ embryos all had gross structural differences from the stereotypical wild-type and heterozygous lung explants (Fig. 2B,D,F, Fig. S1). By E13.5, isolated embryos no longer demonstrated obvious outward chest wall displacements and it was difficult to differentiate *Wt1* null from wild-type or heterozygous embryos based on the chest cavity appearance. However, in E13.5 *Wt1* null embryos, fluid accumulation was still present, often in the lower abdominal cavity to varying extents (Fig. 2G,I,K). Explanted lungs from null embryos similarly had gross and more extensive structural differences from normal lung stereotypy (Fig. 2H,J,L), and 'pinched' lobes (Fig. 2J) were observed often on E13.5 lungs. These pinched areas are consistent with closure of the diaphragm at E13.5 and herniation of the lung into the abdominal cavity. Although herniation of the lung into the abdominal cavity is opposite to that observed in the human CDH condition, it is 'normal' in the *Wt1* knockout model of CDH (Carmona et al., 2016; Kreidberg et al., 1993; Paris et al., 2015).

To understand better the gross deviations in lung morphology, we immunostained lung explants at early gestational stages using E-cadherin (cadherin 1) as a marker to visualize and quantify the airway branch architecture (Fig. S1). At E11.5, no gross morphological branching defects were obvious relative to littermate controls, and normal lobe specification had occurred. By E12.5, alterations in epithelial branching architecture were visible in *Wt1*

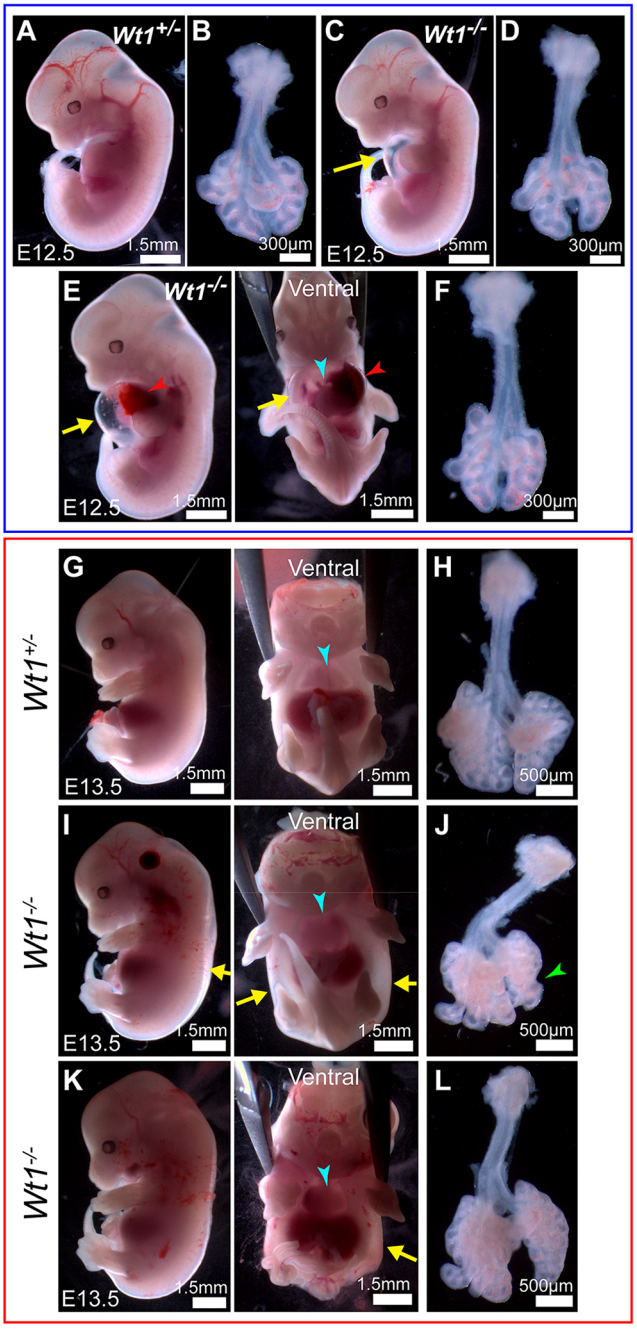

Fig. 2. Intrafetal fluid accumulation within the body cavity is visible starting at E12.5 in $Wt1^{-/-}$ mutant embryos. (A-F) Representative E12.5 embryos in which pleural effusion was identified by distention (yellow arrows) of the pleural cavity in $Wt1^{-/-}$ embryos (A versus C,E). (B,D,F) The corresponding lung tissue isolated from the embryos in A,C,E, respectively. Varying degrees of edema resulted (C versus E) and many embryos displayed blood in the pleural fluid (red arrowheads). From the ventral view the heart is visible (blue arrowhead). All E12.5 embryos are littermates. (G-L) Representative E13.5 embryos demonstrate chest wall displacement is no longer obvious in any genotype (G,I,K). Generalized ascites are visible in null embryos (I,K, yellow arrows), and are present to varying degrees. From the ventral view the heart is visible (blue arrowheads). (H,J,L) The corresponding lung tissue isolated from the embryos in G,I,K, respectively. Some lungs demonstrated the 'pinching in' phenotype (J, green arrowhead). All E13.5 embryos are littermates.

Development (2021) 148, dev199460. doi:10.1242/dev.199460

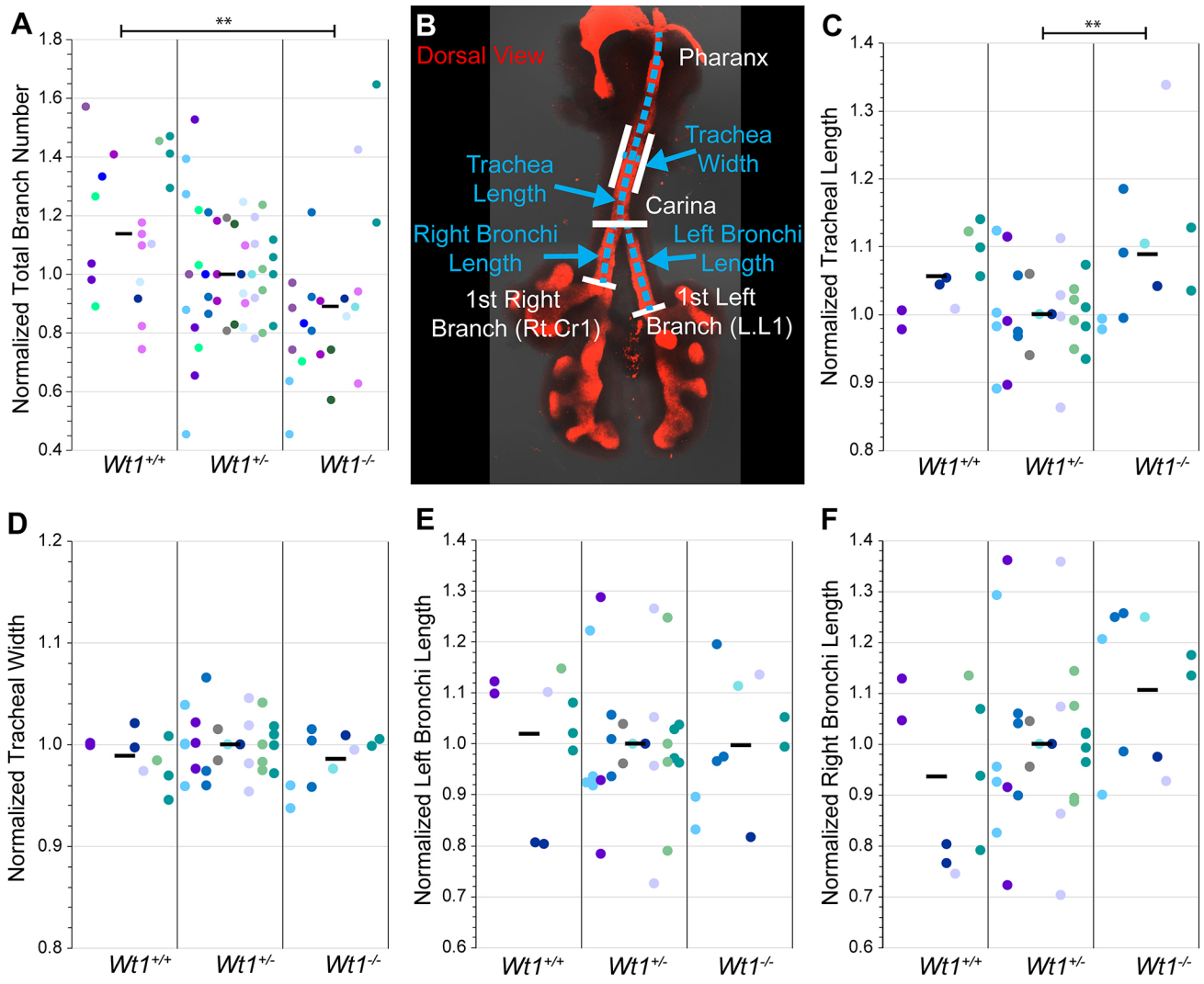

Fig. 3. *Wt1*$^{-/-}$ lungs exhibit pulmonary hypoplasia. (A) Total branch numbers of E12.5 lungs were quantified and normalized to the average heterozygous branch number per uterus. (B) Schematic illustrating morphometric measurements. (C-F) Lungs were quantified for tracheal length (C), tracheal width (D), and left (E) and right (F) bronchi lengths with each value measured as indicated in the schematic (B). Measurements were normalized to the average heterozygous value for each uterus. **P<0.01. Individual data points represent individual lung explants measured, and colors of data points indicate littermates to allow for comparison within a single uterus, and across genotypes for each uterus. Black horizontal lines indicate mean value of data points shown.

null lungs compared with wild-type and heterozygous littermates, which otherwise followed the typical conserved stereotypy (Metzger et al., 2008). Overall, null lungs had a narrower, more elongated morphology along with a more dorsal-ventral flattened structure. Consistent with the phenotype of CDH, *Wt1*$^{-/-}$ lungs presented with pulmonary hypoplasia with on average fewer epithelial branches compared with heterozygous lungs, and significantly fewer epithelial branches compared with *Wt1*$^{+/+}$ littermates (Fig. 3A).

Apart from the noted differences in growth in *Wt1*$^{-/-}$ lungs, perhaps the best description of the gross lung morphology is that they were reliably inconsistent in the patterns of their altered architecture (Fig. S2). Branches were often observed growing in atypical orientations, but not in any consistent pattern between embryos, matching the CDH condition of variable penetration of phenotype. To understand some of the main sources of variation observed across all *Wt1*$^{-/-}$ lungs, we quantified the main architectural alterations in epithelial branching, including tracheal and main bronchi lengths, tracheal width, and branching angles of the medial and accessory lobes (Fig. 3B). To account for any slight gestational differences between individual litters for quantitative measurements, each measurement was normalized to the average heterozygous littermate value within each uterus. *Wt1*$^{-/-}$ lungs had significantly longer tracheas compared with heterozygous littermates, but this was not statistically significant compared with wild-type littermates (Fig. 3C, Fig. S1B,C). No differences were found in tracheal width (Fig. 3D) nor in the length of the left mainstem bronchi (Fig. 3E); however, *Wt1*$^{-/-}$ right bronchi lengths were on average longer than both *Wt1*$^{+/+}$ and *Wt1*$^{+/-}$ right bronchi, but this was not statistically significant (Fig. 3F).

The most common observable break from lung stereotypy across all *Wt1*$^{-/-}$ lungs was the abnormal orientation of the medial lobe. The accessory lobe angle was significantly larger in the null and wild-type lungs compared with heterozygous lungs (Fig. 4A,B). Deviations of the medial lobe angle in null lungs were extreme, which is not surprising given this deviation was grossly observable prior to quantification (Fig. 4A,C). The medial lobe angle was significantly increased in heterozygous lungs compared with wild type, and further

Development (2021) 148, dev199460. doi:10.1242/dev.199460

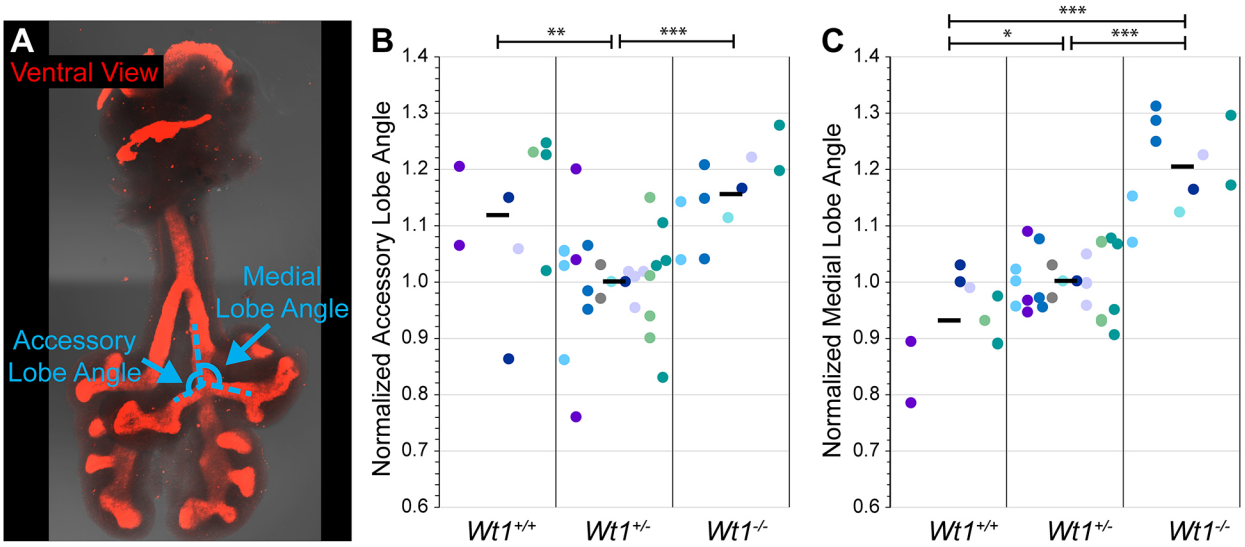

Fig. 4. *Wt1*$^{-/-}$ lungs have abnormal accessory and medial lobe angles. (A) Schematic illustrating morphometric measurements of branch angles. (B,C) Lungs were quantified for accessory (B) and medial (C) lobe angles. Measurements were normalized to the average heterozygous value for each uterus. **P*<0.05, ***P*<0.01, ****P*<0.001. Individual data points represent individual lung explants measured and colors of data points indicate littermates to allow for comparison within a single uterus, and across genotypes for each uterus. Black horizontal lines indicate mean value of data points shown.

significantly increased in null lungs compared with both heterozygous and wild-type tissues. This feature seemed to follow a trend with the number of copies of *Wt1* present, with *Wt1*$^{+/-}$ lungs having an intermediate phenotype between *Wt1*$^{+/+}$ and *Wt1*$^{-/-}$ lungs. The increased medial and accessory lobe angles indicate a mispositioning of these lobes distally relative to the carina and a more flattened dorsal-ventral overall lung morphology.

Expression of key morphological genes were decreased in the *Wt1* null model

To quantify the changes in WT1 in early gestation observed via immunofluorescence, we used tungsten needles to mechanically isolate distal lung epithelium and mesothelium from E11.5, E12.5 and E13.5 CD-1 embryos and performed qPCR. As expected, the lung epithelium showed no expression of *Wt1*, and mesothelial *Wt1* expression increased with gestational age (Fig. S3A). In considering downstream targets of WT1 in the lung, *Fgf9* is one of the few genes known to be expressed by the lung mesothelium (Colvin et al., 1999) and studies have demonstrated that *Fgf9* can act downstream of *Wt1* in the heart epicardium (Guadix et al., 2011). Therefore, we assayed for *Fgf9* expression in our epithelial and mesothelial tissue isolates and determined that *Fgf9* expression parallels that of *Wt1*, and similarly increases with gestational age in early lung development (Fig. S3B). Additionally, given the changes in branching morphogenesis in our *Wt1*$^{-/-}$ lungs, we examined other specific hallmark genes of lung development, including some related to *Fgf9* expression (*Fgfr2iiic*, *Fgf10*, *Fgfr2iiib*), along with a gene known to be expressed by lung mesothelium (*Aldh1a2*) (Niederreither et al., 2002), and a gene previously linked to deviations from stereotypy (*Spry2*) (Metzger et al., 2008). Interestingly, gene expression changes occurred throughout multiple tissue compartments in the *Wt1* knockout lungs relative to heterozygous and wild-type lungs (Fig. 5A). In *Wt1*$^{-/-}$ lungs, *Fgf9* expression was significantly decreased along with its mesenchymal receptor *Fgfr2iiic*. Similarly, *Fgf10* expression was decreased, but its receptor, *Fgfr2iiib*, which is expressed in the epithelium, was not significantly different. Lastly, expression of *Aldh1a2*, a gene that encodes an essential retinoic acid-processing enzyme, was significantly decreased, and there was no significant difference in expression of *Spry2* between wild-type and null lungs.

Wt1-deficient lungs branch normally in *ex vivo* culture, but do not recover gene expression differences

Because consistent but irregular gross deviations to lung stereotypy and alterations in expression of several key mediators of airway morphogenesis were present in *Wt1* null lungs, we sought to decouple the development of the lung from any well-established defects with diaphragmatic closure in this mouse model. To do this, we cultured E12.5 lung explants on floating membranes at the air-liquid interface and imaged them over 48 h using time-lapse microscopy. Total branch number and branching rate were compared between genotypes. Surprisingly, *Wt1* null lungs branched normally in culture (Fig. 5B). Although the initial lung morphology was different between genotypes, the null lungs had a remarkable recovery of growth during culture, with a greater fold change in branches (Fig. 5C). After culture, there were no significant differences in total branch number (Fig. 5C) between all three genotypes. Similarly, the spontaneous peristaltic contractions of the airway smooth muscle observed in *ex vivo* lung culture were present and unaffected by *Wt1* knockout.

As we were unable to observe obvious differences in growth during *ex vivo* culture of the lungs related to the presence or absence of WT1, we decided to re-assess mRNA levels of the same key growth-associated genes as assayed previously to determine whether expression had changed during culture (Fig. 5D). As expected, *Wt1* relative expression remained significantly different between *Wt1*$^{+/+}$ and *Wt1*$^{-/-}$ lungs after 48 h of culture. However, unexpectedly, after culture the expression of *Wt1* was significantly different between all genotypes. This indicates a shift in expression pattern that suggests that *Wt1* expression decreases as a result of culturing. Following culture, all genes assayed were significantly different between wild-type and null lungs, suggesting that the similar branching of null lungs was not due to recovery of gene expression of these specific growth molecules assayed. In fact, the relative gene expression between wild-type and null lungs did not change at all following culture for many genes, including the

Development (2021) 148, dev199460. doi:10.1242/dev.199460

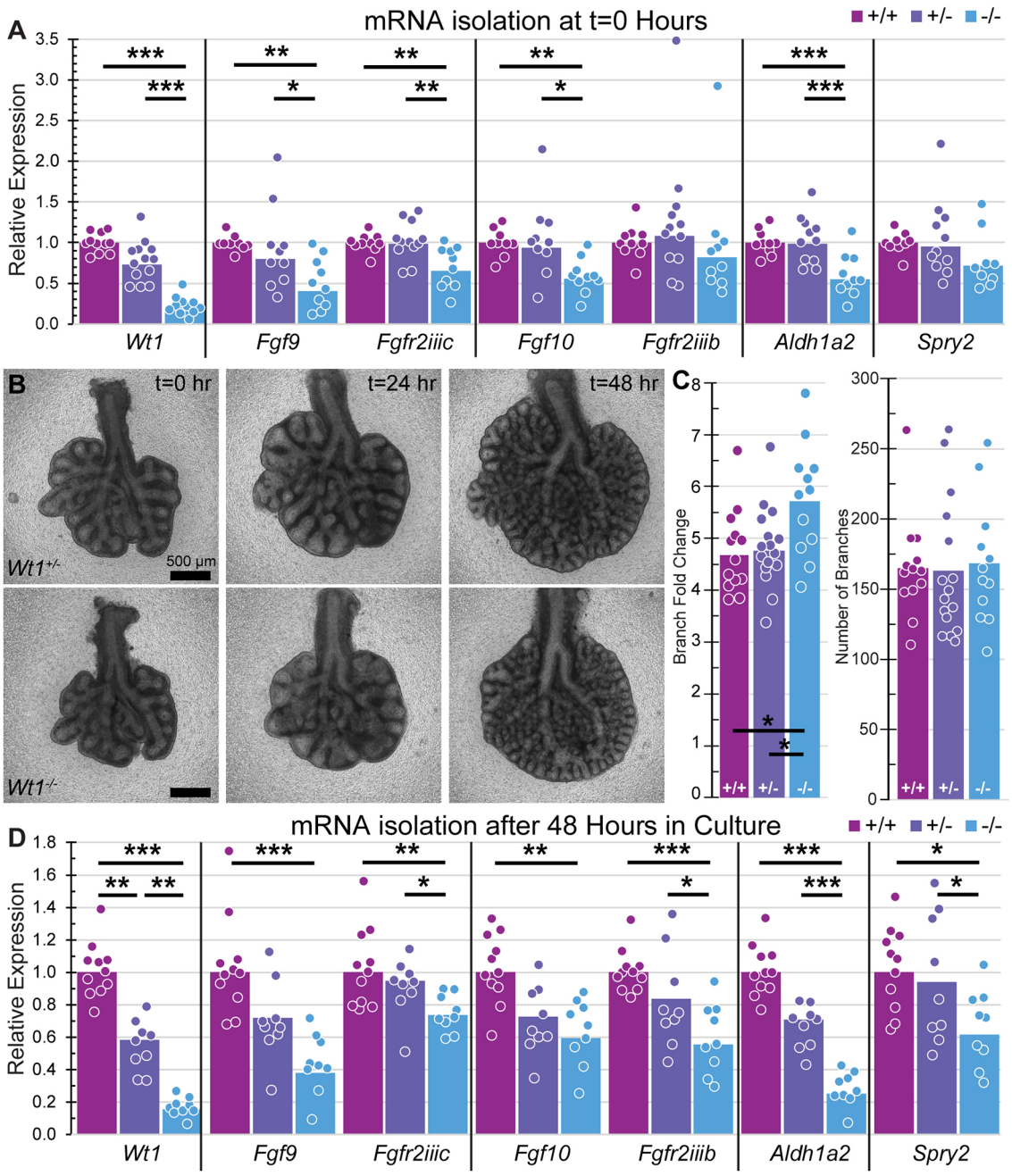

Fig. 5. Gene expression changes of null lungs do not recover after *in vitro* culture. (A) Whole lung mRNA lysates from individual E12.5 lungs at t=0 were analyzed by qPCR. (B) E12.5 lungs were isolated and cultured for 48 h of membrane culture. Branching of $Wt1^{-/-}$ lungs appears comparable to littermate $Wt1^{+/+}$ and $Wt1^{+/-}$ lungs. (C) Branch number was quantified after 48 h and normalized to branch number at 0 h to determine fold change. Total branch number was not significantly different between genotypes after culture. (D) Whole lung mRNA lysates from individual E12.5 lungs at t=48 h of culture were analyzed by qPCR. *P<0.05, **P<0.01, ***P<0.001. Gene expression was normalized to $Wt1^{+/+}$ littermate controls for each uterus. Individual data points represent individual lung explants measured.

relative expression of *Fgf9*, *Fgfr2iiic* and *Fgf10*. Other genes, such as *Fgfr2iiib* and *Aldh1a2*, had further decreased relative expression in the null lungs compared with wild-type lungs after culture.

To extend our end-point analysis of branching following culture, we also investigated the dynamics of branching to determine whether overall growth of the null lungs was comparable to the other genotypes, and if stereotypy was conserved. Using time-lapse microscopy of the lungs in culture, we quantified the rate of branch extension (Fig. 6A). To account for any spatial variability, we analyzed branch growth rate within branch families (parent and daughter branches appearing over the time-lapse period), families within the same lobe, and between lungs of the same genotype. The slope of the linear regression of branch length (L-L_0) as a function of time (t-$t_{initiation}$) was taken as the branch extension rate (Fig. 6B,C). Branch rates as a function of time within a branch family and between branches on different lobes were similar, ranging on average from 5 to 7 µm/h (Fig. 6D-I). Branch extension rates were similar across all genotypes at the locations assessed, with $Wt1^{-/-}$ lungs having extension rates on par with littermate controls. Only for the L1.1 family was the null branch extension rate significantly

Development (2021) 148, dev199460. doi:10.1242/dev.199460

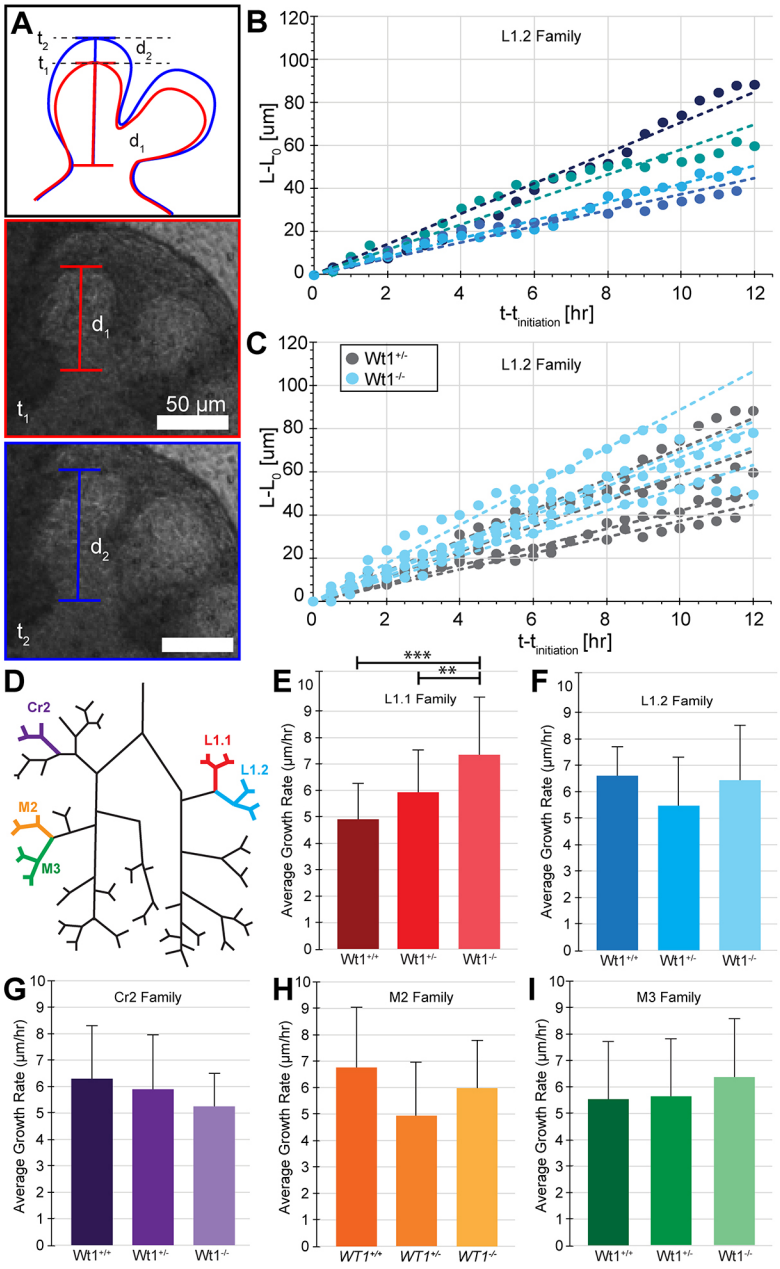

Fig. 6. Upon removal from the chest cavity, branching capacity is recovered in *Wt1*$^{-/-}$ lungs. (A) Branch length was measured from the neck of a branch to the most distal linear point of a branch tip (d_1 d_2) at different times throughout culture (t_1 t_2). (B) Example linear growth (L-L_0) throughout culture for a single branch family on a *Wt1*$^{+/-}$ lung. Each color represents a separate branch. Growth rate was determined from the best-fit line for each branch (dashed lines). (C) Example linear growth throughout culture for a littermate *Wt1*$^{-/-}$ lung (blue data points) for the same branch family and overlaid over the plot shown in B (gray data points). (D) Schematic showing the various branch families used to compare branching rates. (E-I) Average branching rate for each branch family. Color of plot corresponds to color of branch family in schematic (D). Mean±s.d. $^{**}P<0.01$, $^{***}P<0.001$, $n\geq3$ lungs per genotype, $n=3$ uteri.

higher than that of wild-type and heterozygous lungs (Fig. 6E). There were no significant differences between *Wt1*$^{-/-}$ and *Wt1*$^{+/+}$ lungs for all other measurements (Fig. 6D,F-I). Importantly, branch lengths were also not significantly different between genotypes, and branching architecture was conserved, indicating that stereotypical branching occurred in null lungs. These data demonstrate that even with initial differences in lung morphology and gene expression, once removed from the embryo *Wt1*$^{-/-}$ lungs have the capability to branch normally.

Loss of *Wt1* decreases space in the chest cavity for the developing lung

We sought to understand the spatial relationship of the lung within the chest cavity as normal growth and branching was rescued in *Wt1*$^{-/-}$ lungs when cultured *ex vivo*. Previously, we have shown that lungs alter their growth and gross morphology to fill cavities of different shapes in *ex vivo* culture (Nelson et al., 2017). We hypothesized that some of the gross morphological changes observed in *Wt1*$^{-/-}$ embryos may alter the organization of organs within the chest cavity. To investigate this, we used micro-CT to image embryos *in situ* within the uterus (Fig. 7A-C). Owing to the methods required to process the uterus and embryos for this imaging modality, we were unable to determine embryo genotypes; however, imaging *in situ* was consistent with gross findings from embryos, i.e., intrafetal effusion and altered lung morphology. As such, we could easily identify *Wt1* null embryos but were unable to differentiate *Wt1*$^{+/+}$ from *Wt1*$^{+/-}$ embryos. Therefore, we refer to tissues as WT1(−) for null and Wt1(+) for heterozygous and wild-type embryos, respectively.

Using micro-CT imaging, we were able to quantify the somite stage of each embryo, and the approximate lung stage, which was quantified by grading the degree of branching from 0 to 5 (Fig. S4). Lung stage was found to scale with somite number. Both WT1(+) and WT1(−) had similar lung stages for a given somite number,

Development (2021) 148, dev199460. doi:10.1242/dev.199460

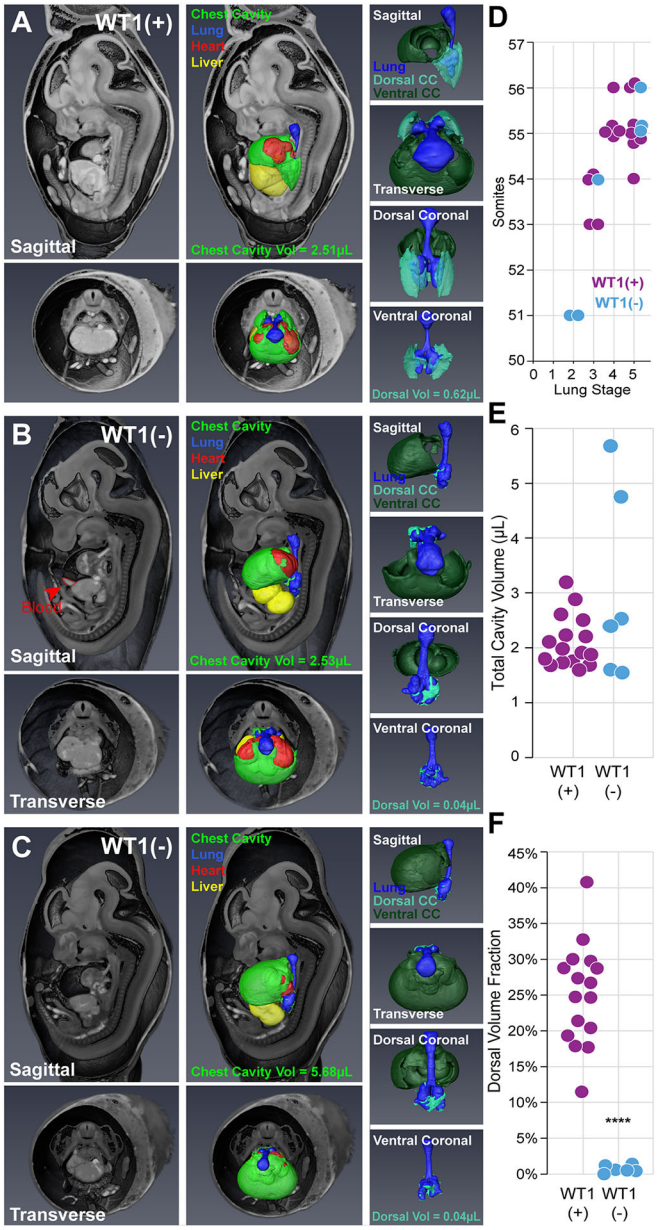

Fig. 7. Dorsal chest cavity volume is absent in *Wt1*$^{-/-}$ embryos. (A-C) Representative E12.5 embryos imaged *in situ* using micro-CT. Organ volumes of interest were segmented, including the chest cavity (green), lung (blue), heart (red) and liver (yellow). The chest cavity was further segmented into a ventral (dark green) and dorsal (mint green) chest cavity. All three embryos shown are littermates. (D) Somites were counted for all embryos analyzed and plotted against the graded lung stage for each embryo. (E) Total volume of the segmented chest cavity for WT1(+) and WT1(−) embryos. (F) The volume fraction of the dorsal chest cavity with respect to the total chest cavity volume as determined by the segmentation analysis for WT1(+) and WT1(−) embryos. *n*=4 uteri, ****P<0.0001. Individual data points represent individual embryos measured.

indicating that the lung stage correlated with the somite age of the embryos, and lungs that appeared gestationally delayed were likely from embryos experiencing global growth delays (Fig. 7D, Fig. S4). We used Amira software to segment areas of interest from the chest cavity, including the open unoccupied chest cavity volume itself, the trachea and lungs, and the heart. These segmented areas were then reconstructed into surfaces for visualization and calculation of volumes (Fig. 7A-C). The chest cavity of E12.5 WT1(+) embryos consisted of a larger ventral space defined between the chest wall and heart (eventual pericardial cavity), connected latterly to a smaller dorsal space (eventual pleural cavity) behind the heart in which the lung grows (Fig. 7A). Reconstruction of this chest cavity volume and the lung revealed a dorsal space much larger than the lungs themselves with space for additional growth. Surprisingly, when WT1(−) embryos were imaged, a dorsal space in the chest cavity could not be easily defined. In these *Wt1* knockout mice the lung boundaries are coincident with the boundaries of the heart, back of the chest cavity wall, and the liver/diaphragm (Movies 1-3). Given the obvious effusions observed grossly in the embryos, this finding was unexpected. In the six *Wt1* knockout embryos that were imaged across four different uteri, the amount of intrafetal effusions varied and thus the total chest cavity volume varied (Fig. 7B,C). Quantification revealed no significant difference in the total chest cavity volume between WT1(+) and WT1(−) embryos (Fig. 7E). However, in WT1(−) embryos, nearly all chest cavity volume and additional fluid was distributed to the ventral compartment, with the

Development (2021) 148, dev199460. doi:10.1242/dev.199460

dorsal volume fraction ranging from 0% to 1.4% of the total cavity volume (Fig. 7F). Additionally, we used micro-CT to examine WT1(−) and WT1(+) embryos at E13.5, the time point of normal closure of the diaphragm (Fig. S5, Movies 4, 5). Similarly, there was a clear absence of any dorsal space in the chest cavity in WT1(−) embryos, compared with an extensive dorsal space for lungs to grow within in WT1(+) embryos. In all E13.5 WT1(−) embryos, the displacement of the medial lobe can be visualized through the right side of the diaphragm, and this portion of the lung was in direct contact with the liver. Multiple embryos also exhibited distal portions of the left lobe that had extended through the left side of the diaphragm into the abdominal cavity. This indicates the presence of a herniation and diaphragmatic defect, consistent with the 'pinching in' phenotype we observe when E13.5 lungs are explanted. Upon segmentation of the diaphragm, we were able to observe holes in the diaphragm through which the lung had herniated (Fig. S5, Table S1, Movies 4, 5).

DISCUSSION

CDH is a common life-threatening congenital birth defect with varying severity and unknown etiology. We sought to understand this condition and the effects on lung development using an established genetic mouse model of CDH, *Wt1* knockout, which recapitulates a CDH-like phenotype. To date, the *Wt1* knockout as a model of CDH has largely been used to investigate the role of WT1 in diaphragm and heart development, but has not been thoroughly examined in the context of the lung, even though WT1 is also present in the lung mesothelium. This is particularly important given the CDH 'dual hit' hypothesis developed using the rodent nitrofen model (Keijzer et al., 2000), whereby alterations in lung morphogenesis are demonstrated before normal closure of the diaphragm, suggesting defects in the lung and diaphragm as a first 'hit', followed by a subsequent 'hit' to the lung with herniation of organs through the diaphragm. In this study, we show localization of WT1 in the lung mesothelium at gestational stages prior to or during diaphragmatic closure to indicate regions that could be affected by WT1. We then knocked out *Wt1* and grossly observed significant intrafetal effusions in all null embryos and changes in lung branching architecture at an early gestational age, E12.5, before diaphragm closure. Analysis of gene expression revealed changes in key mediators of lung branching morphogenesis, including *Fgf9*, *Fgf10* and *Aldh1a2*, a gene encoding an essential enzyme for vitamin A processing that has been shown to be altered in other rodent CDH models. We then cultured *Wt1* knockout lung explants *ex vivo*, to remove any potential confounding effects from the physical *in vivo* environment and diaphragm development. Surprisingly, normal airway branching occurred, with branch number, extension rates, and architecture the same as in wild-type and heterozygous lung explants. Any initial hypoplasia at the start of culture was rescued over 48 h in culture (Figs 5 and 6). This indicated that null lungs still maintained the capacity to branch normally upon isolation from the *in vivo* environment. We then re-examined the genes considered to be essential mediators of branching in the lungs after culture and, unexpectedly, gene expression did not recover, despite recovery of branching morphogenesis. Given the ability of the lung to grow normally *ex vivo* yet have dysregulated morphology and branching hypoplasia when initially removed from the embryo, we used micro-CT to visualize the organization of organs within the chest cavity. We found that lungs of all null embryos were tightly associated with the neighboring tissues with a near absence of space for lung growth in *Wt1* knockout relative to heterozygous or wild-type embryos. This physical constraint likely resulted in the variability and dysregulated branching observed in *Wt1* knockout lungs.

The *Wt1* knockout model has been used previously to study CDH, in which it was observed that null lungs appeared hypoplastic compared with wild-type littermates (Cano et al., 2013; Carmona et al., 2016; Clugston et al., 2006; Kreidberg et al., 1993; Paris et al., 2015). However, lung hypoplasia in these models has only been identified by gross observation of histological sections and has not been rigorously assessed with respect to branch number or somite stage. Our data also seemed to show the same finding of hypoplasia in null lungs compared with wild type (Fig. 3A). However, using micro-CT data, we determined the stage of lung branching by grading the degree of airway branch elaboration (Kadzik et al., 2014; Menshykau et al., 2014; Metzger et al., 2008), as well as the embryonic age by counting somites. When compared between genotypes, WT1(−) and WT1(+) embryos of the same somite stage have lungs of the same graded branch stage (Fig. 7D, Fig. S4). This indicates that null lungs are not hypoplastic due to a specific lung deficit, but rather appear hypoplastic due to a whole embryo gestational delay. This global gestational delay would be consistent with the use of a global genetic knockout that could be affecting overall embryonic growth.

The role WT1 plays within the pleural mesothelium is still unclear. Although some roles for WT1 have been identified in the epicardium and diaphragm, the role in the lung is largely unknown. More recent work has determined that WT1-expressing mesothelium of the lung can act as a multipotent progenitor pool of cells during branching morphogenesis (Cano et al., 2013; Dixit et al., 2013; Karki et al., 2014; Que et al., 2008; von Gise et al., 2016). This is much like the function of the epicardium in heart development (Krainock et al., 2016; von Gise and Pu, 2012), demonstrating the apparent parallels of this tissue layer in different organs. Additionally, the PPFs have been identified as an important tissue structure that is crucial for proper diaphragm development and is covered in a layer of mesothelium. Deletion of genes in the PPFs or the associated mesothelium can produce defects mimicking CDH (Sefton et al., 2018), implicating the importance of this cell type in CDH. In this study, we have identified that deletion of mesothelial *Wt1* induces altered expression of genes within other tissue compartments, including the epithelium (*Fgfr2iiib*, *Spry2*) and mesenchyme (*Fgf10*, *Fgfr2iiic*). This highlights the importance of considering and examining the mesothelium when investigating tissue cross-talk signaling in the developing lung. Of additional importance, for all of the genes assayed, there were no significant gene expression differences between wild-type and heterozygous lungs (Fig. 5A). This is the case even for expression of *Wt1*, indicating that lungs that are heterozygous for *Wt1* are not haploinsufficent. $Wt1^{+/-}$ lungs still had approximately 77% of the *Wt1* expression of wild-type lungs (Fig. 3A). Given that we observe such a robust phenotype in $Wt1^{-/-}$ lungs, these gene expression data correlate with the lack of gross phenotype present in $Wt1^{+/-}$ tissues.

By identifying the gene expression changes in the lung upon knockout of WT1, we attempted to elucidate a role for WT1 during lung development. In normal lungs, we determined that *Fgf9* is expressed mainly by the mesothelium and increases concomitantly with *Wt1* (Fig. S3). Further connecting these two genes, expression of *Fgf9* and its mesenchymal receptor *Fgfr2iiic* are significantly decreased in $Wt1^{-/-}$ lungs, both before and after membrane culture. As WT1 is a transcription factor, it may control expression of several genes, through a variety of pathways. However, our data suggest that *Fgf9* is downstream of *Wt1* expression in the lung, which parallels the same pathway in the epicardium (Guadix et al., 2011). Another

Development (2021) 148, dev199460. doi:10.1242/dev.199460

important FGF expressed by the lung, FGF10, is thought to be responsible for controlling lung branching stereotypy (Bellusci et al., 1997). Studies in the lung have reported that FGF9 could act upstream of FGF10 based on observations of increased *Fgf10* expression by *in situ* hybridization when lung explants were cultured with FGF9 (Del Moral and Warburton, 2010), or when FGF9 was overexpressed in the lung (White et al., 2006). Examining *Fgf10* expression in $Wt1^{-/-}$ lungs reveals significantly decreased expression of *Fgf10* before and after membrane culture, and a slight but not significant decrease of its epithelial expressed receptor *Fgfr2iiib* (Fig. 5A). Our data suggest that WT1 is upstream of *Fgf9* and of *Fgf10*. Given our and these other published results, it is likely that the decrease in *Fgf10* can be attributed to changes in *Fgf9*. As *Fgf9* and *Fgf10* are still expressed with *Wt1* knockout, other factors beyond WT1 are likely also contributing to their expression. Even after membrane culture and apparent recovery of branching, *Fgf9* and *Fgf10* still had significantly decreased expression. This indicates that the decreased *Fgf9* and *Fgf10* gene expression is not due to physical confinement of the $Wt1^{-/-}$ lungs and is likely due to the perturbed WT1 molecular pathway. Additionally, because *Fgf9*, *Fgf10* and *Aldh1a2* gene expression were not recovered after culture, yet lung branching was recovered, these classic lung morphogens are unlikely to be directly responsible for the altered lung morphology observed in the WT1 null model.

The nitrofen rodent model is a teratogenic model of CDH, and is another classic model used to study CDH. Nitrofen has been shown to inhibit the retinoic acid-processing enzyme ALDH1a2 (Clugston et al., 2006; Kling and Schnitzer, 2007; Mey et al., 2003; Nakazawa et al., 2007). Much like WT1, ALDH1a2 is expressed by mesothelial tissues of the pleural cavity; however, it is not clear whether ALDH1a2 interacts with WT1 in the lung. In a diaphragm-specific knockout of *Wt1*, and in previous $Wt1^{-/-}$ studies, immunohistochemical staining demonstrated a lack of ALDH1a2 in the diaphragm and epicardium (Carmona et al., 2016; von Gise et al., 2011), and concluded that *Wt1* acted upstream of ALDH1a2 in these tissues. However, ALDH1a2 was still present in the adjacent lung tissue, which suggested WT1 might act differently in the lung mesothelium. It is difficult to quantify expression using immunohistochemistry; therefore, in our studies we quantified changes in *Aldh1a2* within $Wt1^{-/-}$ lungs by qPCR and found significantly less *Aldh1a2*, but not a complete loss of expression. This is consistent with ALDH1a2 antigen still being detectable in mutant lung tissue as observed in the literature (Carmona et al., 2016; von Gise et al., 2011). Additionally, after we cultured lungs *ex vivo*, *Aldh1a2* is still significantly decreased compared with wild-type and heterozygous lungs (Fig. 5). Together, these data strongly suggest that WT1 is upstream of ALDH1a2 signaling, but likely acts along with other factors to control the retinoic acid pathway in the lung.

In the *Wt1* knockout model, we observed altered positioning and space within the chest cavity, which likely acts as a physical constraint on the developing lungs in WT1(−) embryos. In $Wt1^{-/-}$ embryos, intrafetal effusions were always observed, although the source of the effusion fluid is not clear. Interestingly, in 8.8% of human CDH cases, effusions of varying amounts are observed in the pleural space, pericardial sac, abdomen, or two or more compartments (Jani et al., 2009; Van Mieghem et al., 2012). We measured the volume of the chest cavity by segmentation of our micro-CT images and determined that total free chest cavity volume was variable between Wt1(−) embryos, but not significantly different compared with Wt1(+) embryos (Fig. 7). Instead, a marked shift in the distribution of the chest cavity volume was observed in Wt1(−) embryos, with minimal free space in the dorsal compartment of the chest cavity (eventual pleural cavity). This is supported by previous observations at later gestational ages using histology in this null model (Cano et al., 2013; Kreidberg et al., 1993). By separating the chest cavity into the dorsal region surrounding the lung and the ventral region around the heart, we clearly see that the majority (>98%) of the fluid-filled space is contained in the ventral region of null lungs, where WT1(+) lungs contain about 75% of the total pleural volume ventrally, and 25% in the dorsal region at E12.5. It is worth noting that in our representative segmentations shown of littermate embryos (Fig. 7A-C), one null embryo has approximately the same chest cavity volume as the WT1(+) embryo (Fig. 7A versus 7B), yet the other null embryo has a much larger chest cavity volume (Fig. 7A versus 7C). This indicates that some WT1(−) embryos may have increased fluid in addition to redistributed chest cavity space and demonstrates the consistent CDH trend of variable penetration of the phenotype. However, both null embryos have approximately equivalent dorsal volumes, despite differences in total chest cavity volumes, thus signifying that the lack of dorsal volume is a conserved phenotype in this model. These differences in dorsal lung space are even more pronounced at a later gestational age (E13.5), with a substantial increase in the free space for the lung to grow within wild-type embryos (Fig. S5, Movies 4, 5). This shift in volume ventrally accounts for the gross visible chest distension in $Wt1^{-/-}$ embryos but it remains to be determined whether fluid secretion within the chest cavity or tissue-tissue interactions cause the altered anatomical placement in these embryos.

Although the effusions are an unlikely driver of CDH, they do indicate significant mesothelial dysfunction. As a barrier tissue, the mesothelium separates and lubricates the tissues and spaces within the chest cavity. Interestingly, we note that during lung dissection, $Wt1^{-/-}$ lungs are more difficult to isolate relative to heterozygous and wild-type lungs. The boundary is less clear and can be described as ‘sticky’ with greater effort needed to isolate the lung explant from the dorsal surface of the heart and other surrounding tissues. Previous work has shown that $Wt1^{-/-}$ lungs have decreased laminin staining along the mesothelium (Cano et al., 2013), perhaps contributing to the ‘sticky’ phenotype. Our data indicates that loss of WT1 does not directly affect lung branching morphogenesis *ex vivo* but may alter mesothelial tissue function resulting in increased adhesions to surrounding tissue and altered barrier integrity, thus contributing to effusions. The physical constraint in WT1(−) embryos coupled with the excess adhesions to neighboring tissue may serve as a physical boundary condition that could alter lung branching and growth, particularly in more stochastic patterns. Indeed, using histology data from later in gestation, others have noted that they could not rule out that lung morphology differences may be secondary to abnormal development of the pleural cavities in this mouse model (Cano et al., 2013). This would produce no clear, conserved, obvious defect between individuals, much like observations in CDH animal models and human cases. However, this repositioning of the lung in the chest cavity observed in our micro-CT images of WT1(−) embryos clearly shows a displacement of the medial lobe to the superior surface of the liver before diaphragmatic closure. Herniation of the lung through the diaphragmatic defect down into the abdominal cavity is not the typical herniation pattern observed in human cases of CDH, where the abdominal organs herniate up into the thoracic cavity. Yet, this still raises the

Development (2021) 148, dev199460. doi:10.1242/dev.199460

intriguing possibility that in *Wt1* null embryos the diaphragmatic defect observed in some cases may be the result of closure of the diaphragm around lung branches that are malpositioned and already protruding into the abdominal cavity. Thus, further investigation should be focused on understanding whether the diaphragmatic defect is the result of dysregulation of the development of the diaphragm, or a consequence of anatomical positioning and constraints within the body cavity.

The lack of free space likely contributes to the altered branching architecture and stereotypy changes observed in $Wt1^{-/-}$ lungs. This is consistent with our previous work demonstrating that the shape of the cavity can direct local airway morphogenesis and global lung architecture in *ex vivo* culture (Nelson et al., 2017). In support of this, initial morphological quantifications show that $Wt1^{-/-}$ lungs have medial lobe displacement, overall flattened dorsal-ventral axis, and much longer tracheas for their stage of development, with a tracheal length comparable to the gestationally older wild-type lungs (Fig. 3C-F). These observations are likely due to the observed lack of pleural volume, as this volume represents the space in which the lung is able to grow, thus forcing the lung to develop within the constraint of decreased available space (Fig. 7). Importantly, we observe decreased cavity space and lung defects at an early gestational age that is prior to any organ herniation and normal closure of the diaphragm, supporting the 'dual hit' hypothesis in this model. We can see that the null lungs are still able to continue to branch and elaborate by E13.5 (Fig. 2G-L, Fig. S5), yet any growth delays at E12.5 will presumably be exacerbated with time if the lung continues to have limited space to grow. This is similar to what is observed in the 'second hit' of the nitrofen model whereby decreased pleural space forces further pulmonary hypoplasia (Keijzer et al., 2000). Together, these data support the hypothesis that the lung is not inherently hypoplastic as a result of this genetic perturbation of *Wt1*, and instead the lungs have altered morphology due to the lack of space available within the chest cavity.

Taken together, our evidence points to the importance of the mesothelium and chest cavity as a whole in lung morphogenesis, particularly in the context of CDH. Using this *Wt1* knockout as a genetic model of CDH, we observe changes in pulmonary morphology and altered lung growth at E12.5, prior to typical closure of the diaphragm. This is consistent in appearance with the 'dual hit' hypothesis that was proposed two decades ago. The 'dual hit' hypothesis was based upon information from nitrofen-exposed mice in which pulmonary defects occurred even in the absence of diaphragmatic hernia (Cilley et al., 1997), and in the nitrofen rat model where lung defects preceded formation of a diaphragmatic defect (Keijzer et al., 2000). However, our micro-CT data demonstrates that, rather than a specific pulmonary defect, alterations in the chest cavity distinct from and prior to abdominal herniation can also contribute to the formation of pulmonary and diaphragmatic defects before normal closure of the diaphragm. Although this idea of a 'second hit' due to organ hernia altering the space available for the lung to grow has been appreciated by surgeons and neonatologists for years, it has not previously been demonstrated that the chest cavity may be altered prior to diaphragmatic defect, and might even drive the defect formation. Consistent with our data in the *Wt1* knockout model of CDH, the nitrofen CDH model reports a predictable but variable degree of lung hypoplasia. It would be interesting to determine whether the nitrofen, vitamin A deficiency, or other genetic rodent models of CDH have alterations in the spatial organization of the chest cavity, which could contribute to the early pulmonary and diaphragmatic defects observed.

MATERIALS AND METHODS

Mouse genetics

All mice were maintained and bred in accordance with Animal Use Protocol approved by the Institutional Animal Care and Use Committee at the University of Delaware (AUP #1320). Timed-pregnant mice were bred and separated 12 h later denoted as E0.5. Post sacrifice, embryos were removed from the uteri and dissected in cold PBS supplemented with 1% penicillin/streptomycin (P/S), using fine forceps to extract intact lung explants (Del Moral and Warburton, 2010; Nelson et al., 2017; Varner et al., 2015).

Lungs used to determine WT1 gestational localization were produced via a timed cross between CD-1 female (Charles River Laboratory, strain code 022) and $WT1^{+/GFPCre}$ male mice (The Jackson Laboratory, stock number 010911). As the Cre insertion disrupts endogenous gene function, for simplicity in the main text, $WT1^{+/GFPCre}$ mice were referred to as $WT1^{+/-}$.

Embryos used for null experiments were created via a timed breed by crossing a $WT1^{+/GFPCre}$ (also referred to as $WT1^{+/-}$) male mouse with a $WT1^{+/GFPCre}$ (also referred to as $WT1^{+/-}$) female mouse that was the progeny of a $WT1^{+/GFPCre}$ male backcrossed with a CD-1 female one generation prior. The backcross was used to increase litter size and therefore the likelihood of having all genotypes present as littermate controls. Excess embryonic tissues from the $WT1^{+/-}$ cross were used for genotyping (The Jackson Laboratory, stock number 010911). Lungs were subsequently isolated and either fixed immediately for staining or lysed for mRNA isolation. Embryos used for micro-CT imaging were fixed immediately within the uterus after isolation and therefore were unable to be processed for genotyping analysis.

Imaging and immunostaining

All embryos and lung explants were grossly imaged using a stereomicroscope (Zeiss Axio Discovery.V8). For immunostaining, lung explants were fixed in 4% paraformaldehyde for 30 min at room temperature and incubated in 0.5% Triton X-100 in 1×PBS overnight. Tissues were blocked, incubated in primary antibodies against WT1 (1:500; Abcam, ab89901) or E-cadherin (1:500; Santa Cruz Biotechnology, sc-59778), and subsequently incubated in anti-rabbit or anti-rat secondary antibodies (1:250; Immunoreagents, DkxRt-003-D550NHSX and DkxRb-003-E488NHSX). Antibody staining was performed at room temperature for 2 h or overnight at 4°C. Confocal microscopy was performed using a Zeiss LSM 800. ImageJ was used for all morphometric analysis.

For quantification of lung morphometrics, the trachea was defined as the length from the oropharynx opening to the carina (Fig. 3B). The left and right bronchi were each defined as the length from the carina to the first branch encountered, L.L1 and Rt.Cr1, respectively. The medial and accessory lobe angles were quantified as the angle formed between the midline of the right mainstem bronchi to the midline of the branch forming the medial lobe or the accessory lobe (Fig. 4A).

For time-lapse microscopy, lung explants were cultured at the air-liquid interface on 8 µm Nuclepore TrackEtched membranes (GE Healthcare) in DMEM/F12 (Corning) supplemented with 5% fetal bovine serum and 1% P/S. Imaging was performed using a Zeiss Axio.Observer Z1 inverted microscope and imaged in brightfield every 5 min for 48 h. Linear growth (L-L0) throughout culture for a single branch family was quantified as branch length measured from the neck of a branch to the most distal linear point of a branch tip (Fig. 6A, d_1, d_2) at different times throughout culture (Fig. 6A, t_1, t_2). If a branch bifurcated during culture, the daughter branches were considered separate branches. Growth rate was determined from the best fit line for each branch.

Quantification of gene expression

For determination of gene expression in different tissue layers, lungs were isolated from embryos of timed-pregnant CD-1 mice. Lungs were incubated for 10 min in 10 U/ml neutral protease (Worthington Biochemical Corporation) on ice, and then neutralized for 10 min in 100% fetal bovine serum. Individual tissue compartments, epithelial and mesothelial, were

Development (2021) 148, dev199460. doi:10.1242/dev.199460

collected from the distal region of the lungs by mechanical isolation with fine tungsten needles, and processed for qPCR as described below.

For gene expression quantification in *Wt1*$^{-/-}$ lung explants, lungs were isolated from embryos and only used for qPCR if all three possible genotypes were present in a single uterus. mRNA was collected from individual lung explants (Bioline), and mRNA was stored at −80°C until further processing. qPCR was performed using a standard amplification mix (Bioline) and the following probes (Thermo Fisher Scientific): *Wt1* (Mm01337048), Shh (Mm00436528), Fgf9 (Mm00442795), Fgfr2iiic (Mm01269938), Fgf10 (Mm00433275), Fgfr2iiib (Mm01275521), Aldh1a2 (Mm00501306), Spry2 (Mm00442344), and Rplp0 (Mm00725448) as an internal control. ΔΔCt values were normalized to the wild-type lung values for each uterus for each gene, and average ΔΔCt values of technical replicates were used for statistical analysis. Statistical analysis was performed using GraphPad Prism3. Data were tested for normality and subsequently analyzed with a one-way ANOVA with Tukey post-hoc test to determine significance.

Micro-CT imaging

Entire uteri used for micro-CT imaging were fixed immediately after surgical removal in 4% paraformaldehyde for 24 h while rocking. Uteri were washed with 1×PBS, incubated for ∼17 h in Lugol's iodine solution (Newcomer Supply, 12092), rinsed with 1×PBS, and embedded in 2% agarose (VWR). Embryos were imaged on a Brüker SkyScan 1276 Micro-CT using filter Al 0.25 mm, 2×2 binning, 10 µm pixel size and 0.3° rotation. Images were reconstructed using NRecon (Brüker), and visualized using CTvox (Brüker). Reconstructed images were manually segmented in Amira (Thermo Fisher Scientific) into the free chest cavity volume, lung, heart and liver compartments. Because the partially forming diaphragm was difficult to resolve at E12.5, we segmented the liver and took its superior surface as a marker for the position of the diaphragm. Volume of the segmented objects was quantified using the MaterialStatistics function in Amira. Statistical analysis of volumes was carried out using Prism software by first performing a normality test to confirm that the data were normally distributed. To determine significance, an unpaired two-tailed *t*-test with Welch's correction was utilized as the variances were significantly different. $P<0.05$ was considered significant.

Lung branching quantification and data analysis

For the branching rate analysis, the length of lung branches from the left, cranial and medial lobes was measured every 30 min for the duration of culture to determine the average growth rate for each branch family. The most recent daughter branch for each family was selected at the beginning of culture and tracked until bifurcation, at which point both resultant daughter branches were measured until the subsequent bifurcation or the end of culture (48 h). Branch length was measured using ImageJ, where the beginning of the branch was considered the neck of the parent branch bifurcation and the end of the branch was the most distal edge. Branch length measurements were normalized to the initial length of the branch and plotted with respect to time. Time was measured relative to each branch initiation and the point of the first measurement was considered t=0. The growth rate of each branch was determined based on the line of best fit with a forced intercept through (0,0). Growth rates were reported as the average growth rate for each branch family. All statistical analyses were performed using GraphPad Prism3 software utilizing a Kruskal–Wallis test and Dunn's multiple comparison post-hoc test for significance with $P<0.05$ considered significant.

Acknowledgements

We thank Sean Holly and Richard West for assistance in developing Micro-CT imaging and quantification protocols.

Competing interests

The authors declare no competing or financial interests.

Author contributions

Conceptualization: R.M.G., J.P.G.; Methodology: R.M.G., J.P.G.; Validation: R.M.G.; Formal analysis: R.M.G., L.E.S., J.P.G.; Investigation: R.M.G., L.E.S.; Resources: R.M.G., J.P.G.; Data curation: R.M.G., L.E.S.; Writing - original draft: R.M.G., J.P.G.; Writing - review & editing: R.M.G., L.E.S., J.P.G.; Visualization: R.M.G.; Supervision: J.P.G.; Project administration: J.P.G.; Funding acquisition: R.M.G., L.E.S., J.P.G.

Funding

This work was supported by grants from the National Institutes of Health (R01HL133163, R21ES027962, P20GM103446 and F31HL140781 to R.M.G.) and the National Science Foundation (BMMB1537256 and GRFP1940700 to L.E.S.). Deposited in PMC for release after 12 months.

References

Baptista, M. J., Melo-Rocha, G., Pedrosa, C., Gonzaga, S., Teles, A., Estevão-Costa, J., Areias, J. C., Flake, A. W., Leite-Moreira, A. F. and Correia-Pinto, J. (2005). Antenatal vitamin A administration attenuates lung hypoplasia by interfering with early instead of late determinants of lung underdevelopment in congenital diaphragmatic hernia. *J. Pediatr. Surg.* **40**, 658-665. doi:10.1016/j.jpedsurg.2005.01.034

Bellusci, S., Grindley, J., Emoto, H., Itoh, N. and Hogan, B. L. (1997). Fibroblast growth factor 10 (FGF10) and branching morphogenesis in the embryonic mouse lung. *Development* **124**, 4867-4878. doi:10.1242/dev.124.23.4867

Cano, E., Carmona, R. and Muñoz-Chápuli, R. (2013). Wt1-expressing progenitors contribute to multiple tissues in the developing lung. *Am. J. Physiol. Lung Cell. Mol. Physiol.* **305**, L322-L332. doi:10.1152/ajplung.00424.2012

Carmona, R., Cañete, A., Cano, E., Ariza, L., Rojas, A. and Muñoz-Chápuli, R. (2016). Conditional deletion of WT1 in the septum transversum mesenchyme causes congenital diaphragmatic hernia in mice. *eLife* **5**, e16009. doi:10.7554/eLife.16009

Cilley, R. E., Zgleszewski, S. E., Krummel, T. M. and Chinoy, M. R. (1997). Nitrofen dose-dependent gestational day-specific murine lung hypoplasia and left-sided diaphragmatic hernia. *Am. J. Physiol.* **272**, L362-L371. doi:10.1152/ajplung.1997.272.2.L362

Clugston, R. D., Klattig, J., Englert, C., Clagett-Dame, M., Martinovic, J., Benachi, A. and Greer, J. J. (2006). Teratogen-induced, dietary and genetic models of congenital diaphragmatic hernia share a common mechanism of pathogenesis. *Am. J. Pathol.* **169**, 1541-1549. doi:10.2353/ajpath.2006.060445

Colvin, J. S., Feldman, B., Nadeau, J. H., Goldfarb, M. and Ornitz, D. M. (1999). Genomic organization and embryonic expression of the mouse fibroblast growth factor 9 gene. *Dev. Dyn.* **216**, 72-88. doi:10.1002/(SICI)1097-0177(199909)216:1<72::AID-DVDY9>3.0.CO;2-9

Coste, K., Beurskens, L. W. J. E., Blanc, P., Gallot, D., Delabaere, A., Blanchon, L., Tibboel, D., Labbé, A., Rottier, R. J. and Sapin, V. (2015). Metabolic disturbances of the vitamin A pathway in human diaphragmatic hernia. *Am. J. Physiol. - Lung Cell. Mol. Physiol.* **308**, L147-L157. doi:10.1152/ajplung.00108.2014

Del Moral, P.-M. and Warburton, D. (2010). Explant culture of mouse embryonic whole lung, isolated epithelium, or mesenchyme under chemically defined conditions as a system to evaluate the molecular mechanism of branching morphogenesis and cellular differentiation. *Methods Mol. Biol.* **633**, 71-79. doi:10.1007/978-1-59745-019-5_5

Dingemann, J., Doi, T., Ruttenstock, E. and Puri, P. (2011). Expression of the Wilm's tumor gene WT1 during diaphragmatic development in the nitrofen model for congenital diaphragmatic hernia. *Pediatr. Surg. Int.* **27**, 159-163. doi:10.1007/s00383-010-2795-y

Dixit, R., Ai, X. and Fine, A. (2013). Derivation of lung mesenchymal lineages from the fetal mesothelium requires hedgehog signaling for mesothelial cell entry. *Development* **140**, 4398-4406. doi:10.1242/dev.098079

Donahoe, P. K., Longoni, M. and High, F. A. (2016). polygenic causes of congenital diaphragmatic hernia produce common lung pathologies. *Am. J. Pathol.* **186**, 2532-2543. doi:10.1016/j.ajpath.2016.07.006

Greer, J. J., Babiuk, R. P. and Thebaud, B. (2003). Etiology of congenital diaphragmatic hernia: the retinoid hypothesis. *Pediatr. Res.* **53**, 726-730. doi:10.1203/01.PDR.0000062660.12769.E6

Guadix, J. A., Ruiz-Villalba, A., Lettice, L., Velecela, V., Muñoz-Chápuli, R., Hastie, N. D., Pérez-Pomares, J. M. and Martínez-Estrada, O. M. (2011). Wt1 controls retinoic acid signalling in embryonic epicardium through transcriptional activation of Raldh2. *Development* **138**, 1093-1097. doi:10.1242/dev.044594

Hiriart, E., Deepe, R. and Wessels, A. (2019). Mesothelium and malignant mesothelioma. *J. Dev. Biol.* **7**, 7. doi:10.3390/jdb7020007

Holder, A. M., Klaassens, M., Tibboel, D., de Klein, A., Lee, B. and Scott, D. A. (2007). Genetic factors in congenital diaphragmatic hernia. *Am. J. Hum. Genet.* **80**, 825-845. doi:10.1086/513442

Jani, J. C., Nicolaides, K. H., Gratacós, E., Valencia, C. M., Doné, E., Martinez, J.-M., Gucciardo, L., Cruz, R. and Deprest, J. A. (2009). Severe diaphragmatic hernia treated by fetal endoscopic tracheal occlusion. *Ultrasound Obstet. Gynecol.* **34**, 304-310. doi:10.1002/uog.6450

Kadzik, R. S., Cohen, E. D., Morley, M. P., Stewart, K. M., Lu, M. M. and Morrisey, E. E. (2014). Wnt ligand/Frizzled 2 receptor signaling regulates tube shape and branch-point formation in the lung through control of epithelial cell shape. *Proc. Natl. Acad. Sci. USA* **111**, 12444-12449. doi:10.1073/pnas.1406639111

Kardon, G., Ackerman, K. G., McCulley, D. J., Shen, Y., Wynn, J., Shang, L., Bogenschutz, E., Sun, X. and Chung, W. K. (2017). Congenital diaphragmatic hernias: from genes to mechanisms to therapies. *Dis. Model. Mech.* **10**, 955-970. doi:10.1242/dmm.028365

Karki, S., Surolia, R., Hock, T. D., Guroji, P., Zolak, J. S., Duggal, R., Ye, T., Thannickal, V. J. and Antony, V. B. (2014). Wilms' tumor 1 (Wt1) regulates pleural mesothelial cell plasticity and transition into myofibroblasts in idiopathic pulmonary fibrosis. *FASEB J.* **28**, 1122-1131. doi:10.1096/fj.13-236828

Keijzer, R., Liu, J., Deimling, J., Tibboel, D. and Post, M. (2000). Dual-hit hypothesis explains pulmonary hypoplasia in the nitrofen model of congenital diaphragmatic hernia. *Am. J. Pathol.* **156**, 1299-1306. doi:10.1016/S0002-9440(10)65000-6

Kling, D. E. and Schnitzer, J. J. (2007). Vitamin A deficiency (VAD), teratogenic, and surgical models of congenital diaphragmatic hernia (CDH). *Am. J. Med. Genet. C Semin. Med. Genet.* **145C**, 139-157. doi:10.1002/ajmg.c.30129

Krainock, M., Toubat, O., Danopoulos, S., Beckham, A., Warburton, D. and Kim, R. (2016). Epicardial epithelial-to-mesenchymal transition in heart development and disease. *J. Clin. Med.* **5**, 27. doi:10.3390/jcm5020027

Kreidberg, J. A., Sariola, H., Loring, J. M., Maeda, M., Pelletier, J., Housman, D. and Jaenisch, R. (1993). WT-1 is required for early kidney development. *Cell* **74**, 679-691. doi:10.1016/0092-8674(93)90515-R

Malpel, S., Mendelsohn, C. and Cardoso, W. V. (2000). Regulation of retinoic acid signaling during lung morphogenesis. *Development* **127**, 3057-3067. doi:10.1242/dev.127.14.3057

Menshykau, D., Blanc, P., Unal, E., Sapin, V. and Iber, D. (2014). An interplay of geometry and signaling enables robust lung branching morphogenesis. *Development* **141**, 4526-4536. doi:10.1242/dev.116202

Merrell, A. J., Ellis, B. J., Fox, Z. D., Lawson, J. A., Weiss, J. A. and Kardon, G. (2015). Muscle connective tissue controls development of the diaphragm and is a source of congenital diaphragmatic hernias. *Nat. Genet.* **47**, 496-504. doi:10.1038/ng.3250

Metzger, R. J., Klein, O. D., Martin, G. R. and Krasnow, M. A. (2008). The branching programme of mouse lung development. *Nature* **453**, 745-750. doi:10.1038/nature07005

Mey, J., Babiuk, R. P., Clugston, R., Zhang, W. and Greer, J. J. (2003). Retinal dehydrogenase-2 is inhibited by compounds that induce congenital diaphragmatic hernias in rodents. *Am. J. Pathol.* **162**, 673-679. doi:10.1016/S0002-9440(10)63861-8

Montedonico, S., Nakazawa, N. and Puri, P. (2008). Congenital diaphragmatic hernia and retinoids: searching for an etiology. *Pediatr. Surg. Int.* **24**, 755-761. doi:10.1007/s00383-008-2140-x

Nakazawa, N., Takayasu, H., Montedonico, S. and Puri, P. (2007). Altered regulation of retinoic acid synthesis in nitrofen-induced hypoplastic lung. *Pediatr. Surg. Int.* **23**, 391-396. doi:10.1007/s00383-006-1848-8

Nelson, C. M., Gleghorn, J. P., Pang, M.-F., Jaslove, J. M., Goodwin, K., Varner, V. D., Miller, E., Radisky, D. C. and Stone, H. A. (2017). Microfluidic chest cavities reveal that transmural pressure controls the rate of lung development. *Development* **144**, 4328-4335. doi:10.1242/dev.154823

Niederreither, K., Fraulob, V., Garnier, J.-M., Chambon, P. and Dollé, P. (2002). Differential expression of retinoic acid-synthesizing (RALDH) enzymes during fetal development and organ differentiation in the mouse. *Mech. Dev.* **110**, 165-171. doi:10.1016/S0925-4773(01)00561-5

Norden, J., Grieskamp, T., Christoffels, V. M., Moorman, A. F. M. and Kispert, A. (2012). Partial absence of pleuropericardial membranes in Tbx18- and Wt1-deficient mice. *PLoS ONE* **7**, e45100. doi:10.1371/journal.pone.0045100

Paris, N. D., Coles, G. L. and Ackerman, K. G. (2015). Wt1 and β-catenin cooperatively regulate diaphragm development in the mouse. *Dev. Biol.* **407**, 40-56. doi:10.1016/j.ydbio.2015.08.009

Que, J., Wilm, B., Hasegawa, H., Wang, F., Bader, D. and Hogan, B. L. M. (2008). Mesothelium contributes to vascular smooth muscle and mesenchyme during lung development. *Proc. Natl. Acad. Sci. USA* **105**, 16626-16630. doi:10.1073/pnas.0808649105

Russell, M. K., Longoni, M., Wells, J., Maalouf, F. I., Tracy, A. A., Loscertales, M., Ackerman, K. G., Pober, B. R., Lage, K., Bult, C. J. et al. (2012). Congenital diaphragmatic hernia candidate genes derived from embryonic transcriptomes. *Proc. Natl. Acad. Sci. USA* **109**, 2978-2983. doi:10.1073/pnas.1121621109

Sefton, E. M., Gallardo, M. and Kardon, G. (2018). Developmental origin and morphogenesis of the diaphragm, an essential mammalian muscle. *Dev. Biol.* **440**, 64-73. doi:10.1016/j.ydbio.2018.04.010

Van Mieghem, T., Cruz-Martinez, R., Allegaert, K., Dekoninck, P., Castanon, M., Sandaite, I., Claus, F., Devlieger, R., Gratacos, E. and Deprest, J. (2012). Outcome of fetuses with congenital diaphragmatic hernia and associated intrafetal fluid effusions managed in the era of fetal surgery. *Ultrasound Obstet. Gynecol.* **39**, 50-55. doi:10.1002/uog.10097

Varner, V. D., Gleghorn, J. P., Miller, E., Radisky, D. C. and Nelson, C. M. (2015). Mechanically patterning the embryonic airway epithelium. *Proc. Natl. Acad. Sci. USA* **112**, 9230-9235. doi:10.1073/pnas.1504102112

von Gise, A. and Pu, W. T. (2012). Endocardial and epicardial epithelial to mesenchymal transitions in heart development and disease. *Circ. Res.* **110**, 1628-1645. doi:10.1161/CIRCRESAHA.111.259960

von Gise, A., Zhou, B., Honor, L. B., Ma, Q., Petryk, A. and Pu, W. T. (2011). WT1 regulates epicardial epithelial to mesenchymal transition through β-catenin and retinoic acid signaling pathways. *Dev. Biol.* **356**, 421-431. doi:10.1016/j.ydbio.2011.05.668

von Gise, A., Stevens, S. M., Honor, L. B., Oh, J. H., Gao, C., Zhou, B. and Pu, W. T. (2016). Contribution of Fetal, but not adult, pulmonary mesothelium to mesenchymal lineages in lung homeostasis and fibrosis. *Am. J. Respir. Cell Mol. Biol.* **54**, 222-230. doi:10.1165/rcmb.2014-0461OC

White, A. C., Xu, J., Yin, Y., Smith, C., Schmid, G. and Ornitz, D. M. (2006). FGF9 and SHH signaling coordinate lung growth and development through regulation of distinct mesenchymal domains. *Development* **133**, 1507-1517. doi:10.1242/dev.02313

Yu, L., Sawle, A. D., Wynn, J., Aspelund, G., Stolar, C. J., Arkovitz, M. S., Potoka, D., Azarow, K. S., Mychaliska, G. B., Shen, Y. et al. (2015). Increased burden of de novo predicted deleterious variants in complex congenital diaphragmatic hernia. *Hum. Mol. Genet.* **24**, 4764-4773. doi:10.1093/hmg/ddv196

Yu, L., Hernan, R. R., Wynn, J. and Chung, W. K. (2019). The influence of genetics in congenital diaphragmatic hernia. *Semin. Perinatol.* **44**, 151169. doi:10.1053/j.semperi.2019.07.008

Supplemental Information

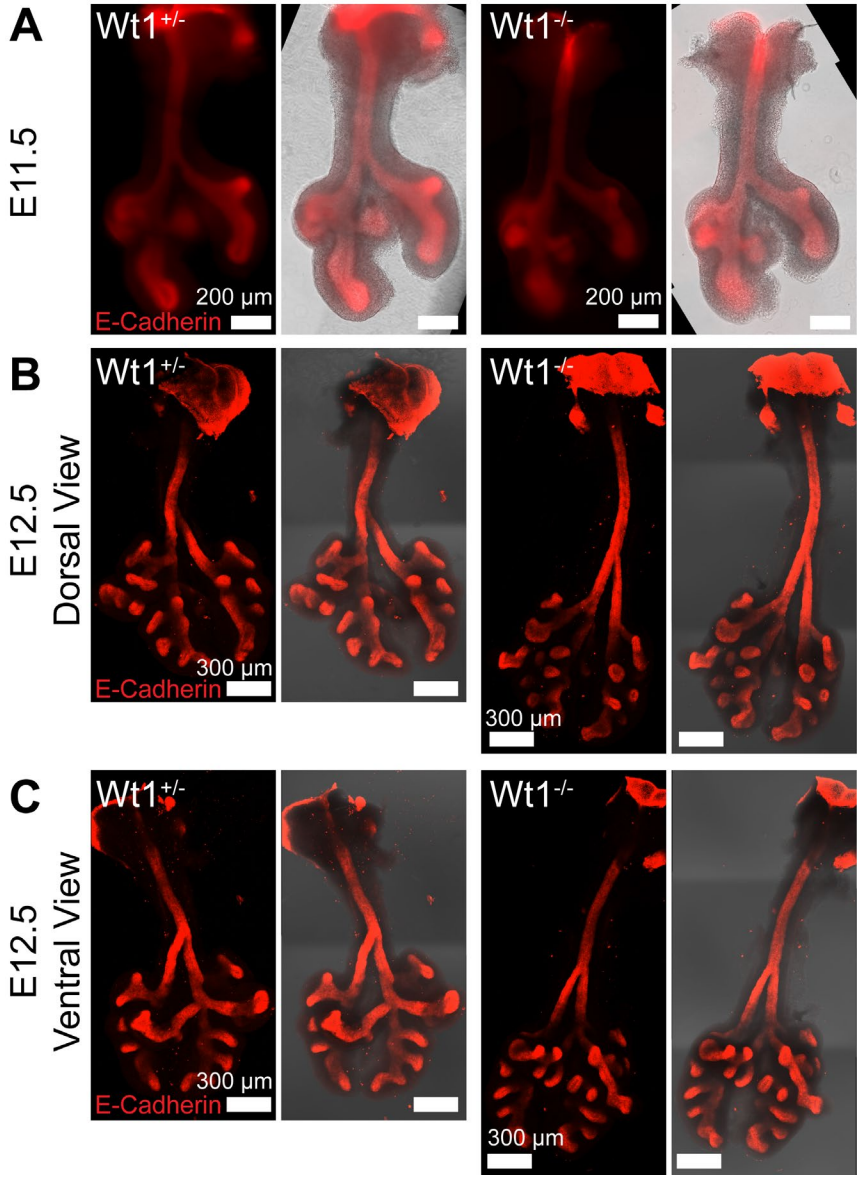

Figure S1: Gross morphology of lungs isolated from *Wt1*$^{-/-}$ embryos indicates early branching defects present. A) Representative E11.5 *Wt1*$^{+/-}$ and *Wt1*$^{-/-}$ lungs stained for E-Cadherin. **B, C)** Representative E12.5 *Wt1*$^{+/-}$ and *Wt1*$^{-/-}$ lungs stained for E-Cadherin shown imaged via the dorsal (B) or ventral (C) perspective. Lung explants for each gestation are littermates. All images shown are maximum intensity projections of confocal z-stacks.

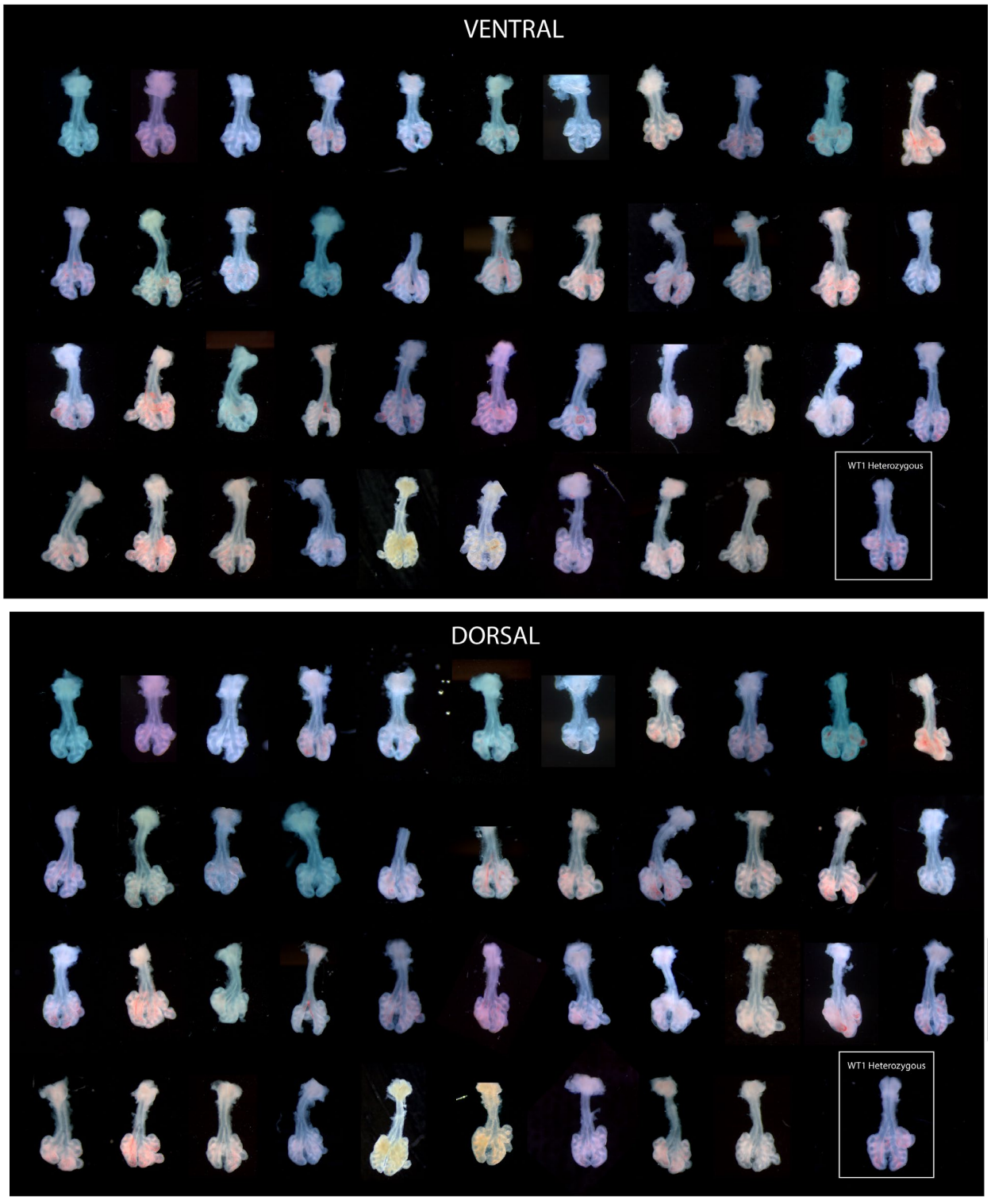

Figure S2: Lung morphology of *Wt1* Null lungs is consistently inconsistent. Gross morphology of *Wt1*$^{-/-}$ lungs imaged via the ventral or dorsal orientation demonstrate the myriad of branching morphologies possible in the null mutant. All morphologies deviate from stereotypy, but with different deviations present in each mutant lung. Common morphological deviations were quantified in Figs 3, 4.

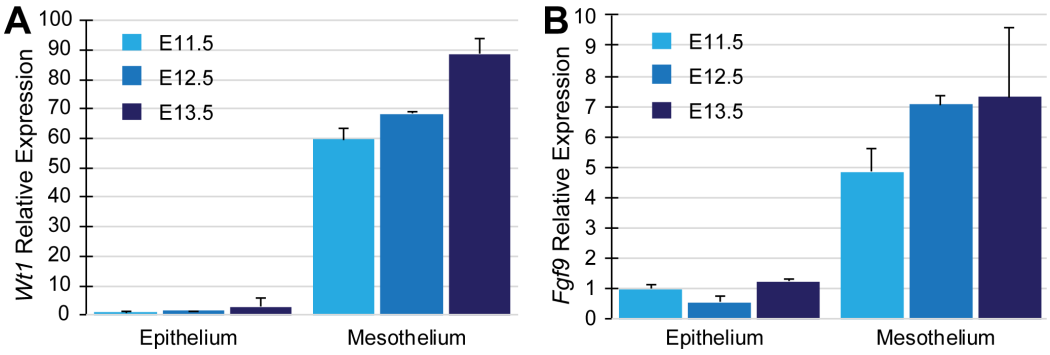

Figure S3: Tissue specific expression of *Wt1* and *Fgf9* changes with gestational age of the tissue. A-B) Individual tissues layers of epithelium and mesothelium were isolated from CD-1 mouse lungs from various gestational ages and assayed for expression of *Wt1* (A) or *Fgf9* (B). mean±SD. Gene expression was normalized to E11.5 epithelial expression levels per gene.

A

Grading Scale of Lung Development

0 - presence of L1-L3	L1 not bi-furcated	L2 not bi-furcated
1 - presence of L1-L4	L1 not bi-furcated	L2 not bi-furcated
2 - presence of L1-L4	L1 bi-furcated	L2 not bi-furcated
3 - presence of L1-L5	L1 bi-furcated	L2 not bi-furcated
4 - presence of L1-L5	L1 bi-furcated	L2 bi-furcated
5 - presence of L1-L6	L1 bi-furcated	L2 bi-furcated

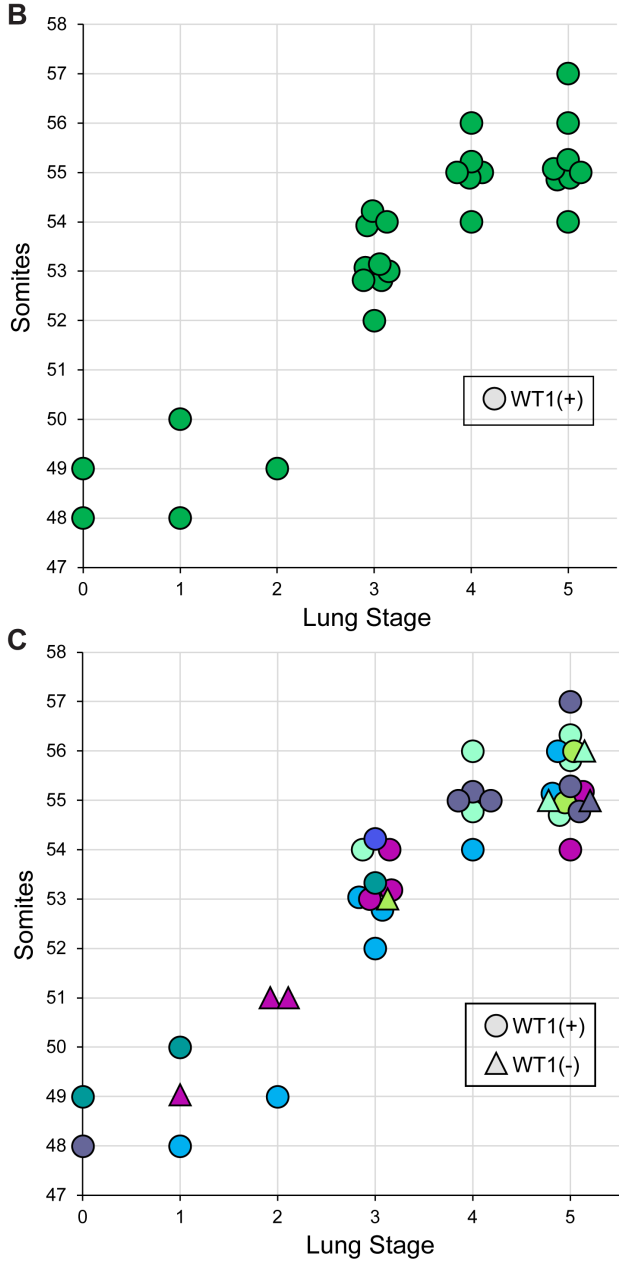

Figure S4: Somites correlate with graded lung stage. A) Metrics used to grade the degree of lung development in E12.5 embryos from WT1 litters **B)** Somites were counted for all WT1(+) embryos analyzed in Fig. 7 and any embryos from uteri without WT1(-) embryos and plotted against the graded lung stage for each embryo. **C)** Somites were counted for all WT1(+) and WT1 (-) embryos plotted against the graded lung stage for each embryo with the varying colors to indicate littermates. n=7 uteri, n=1-8 embryos/uteri

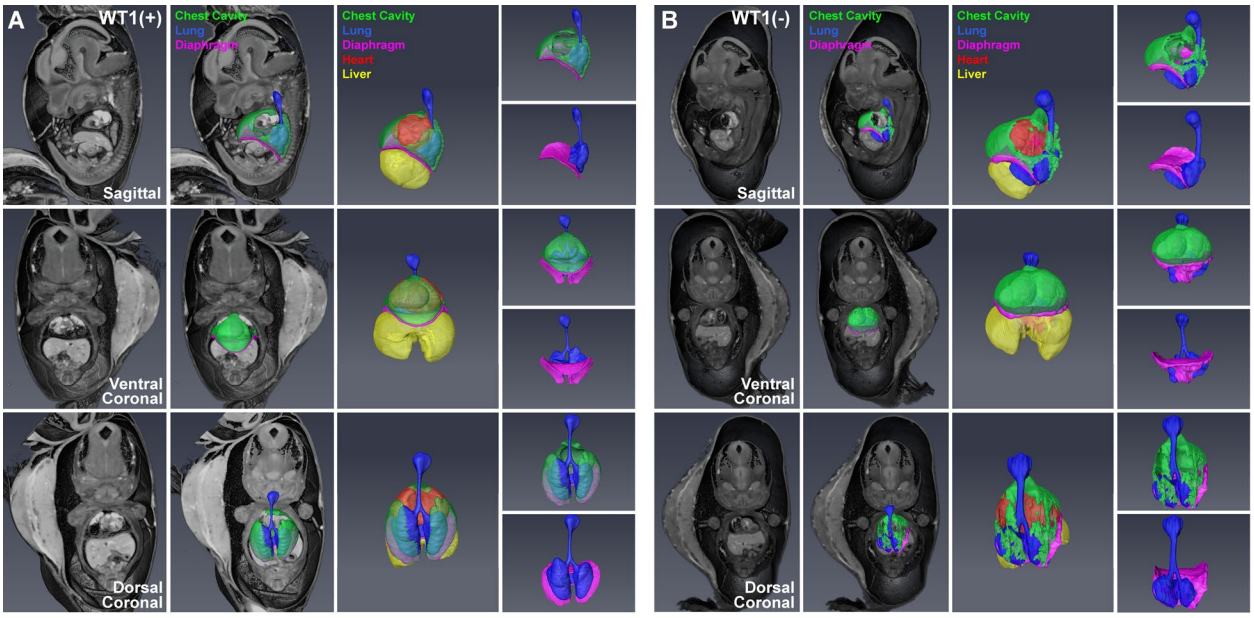

Figure S5: WT1(-) embryos have diaphragmatic defects visible via micro-CT. By E13.5, the diaphragm should be closed with two holes present to allow for the esophagus and descending aorta to pass through. Representative E13.5 littermate embryos were imaged *in situ* via micro-CT, and organs of interest were segmented using Amira. **A-B)** WT1(+) embryos display a large chest cavity volume surrounding the lung which is largely reduced in WT1(-) embryos, consistent with what is observed at E12.5. The morphological differences of the lung are also apparent in the WT1(-) embryo. Two additional large holes are present in dorsal region of the WT1(-) diaphragm, and portions of both the left lung and right lung can be observed growing on the underside of the diaphragm through these diaphragmatic defects. These renderings can also be observed in in Supplemental Movies 4 and 5.

Table S1: E13.5 Incidence of diaphragmatic defect as assessed via micro-CT

Left Sided Posterior Defect Only	Right Sided Posterior Defect Only	Bilateral Posterior Defect
2/10	1/10	7/10

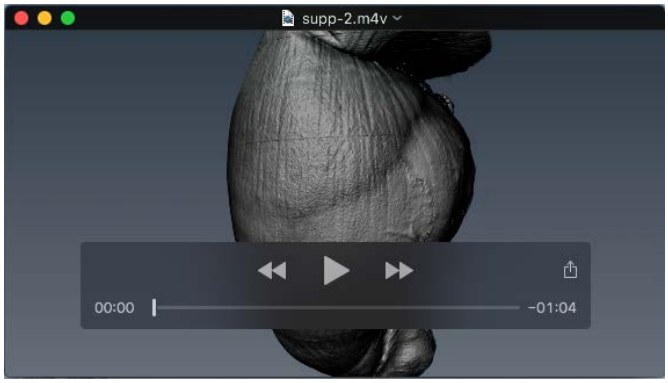

Movie 1: WT1(+) E12.5 embryo imaged *in situ* via micro-CT with Amira segmentation of key volumes. This rendering is also shown in Figure 7A. Note the dorsal volume of the chest cavity in which the lung is growing.

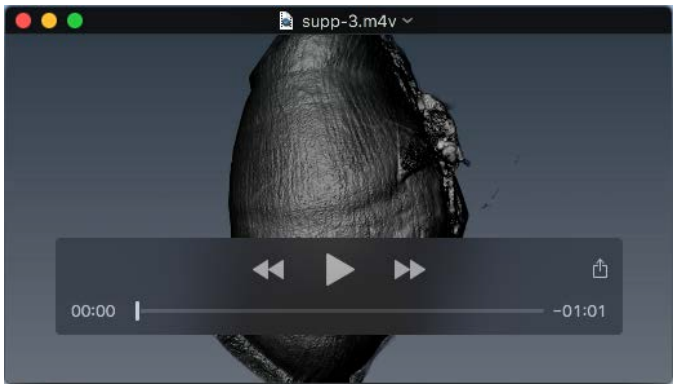

Movie 2: WT1(-) E12.5 embryo imaged *in situ* via micro-CT with Amira segmentation of key volumes. This rendering is also shown in Figure 7B. Note the lack of dorsal volume creating a confined growth environment. The total cavity volume in this embryo is equal to the total cavity volume in the WT1(+) embryo shown in Figure 7A and Movie 1, indicating dorsal-ventral cavity volume redistribution.

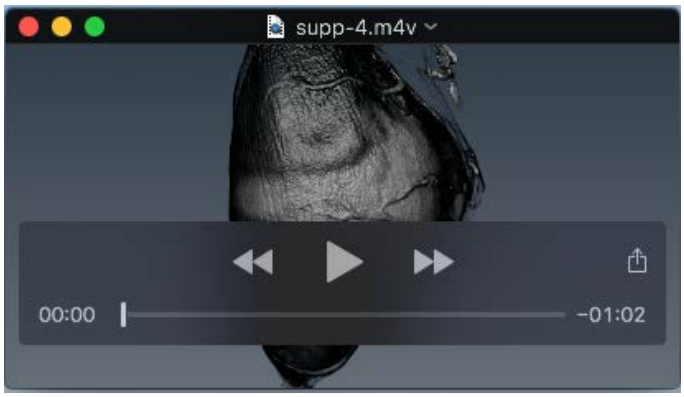

Movie 3: WT1(-) E12.5 embryo imaged *in situ* via micro-CT with Amira segmentation of key volumes. This rendering is also shown in Figure 7C. Note the lack of dorsal volume creating a confined growth environment. The total cavity volume in this embryo is almost double that of the WT1(-) embryo shown in Figure 7B and Movie 2, yet the dorsal volume is equal indicating increased secretion and dorsal-ventral cavity volume redistribution.

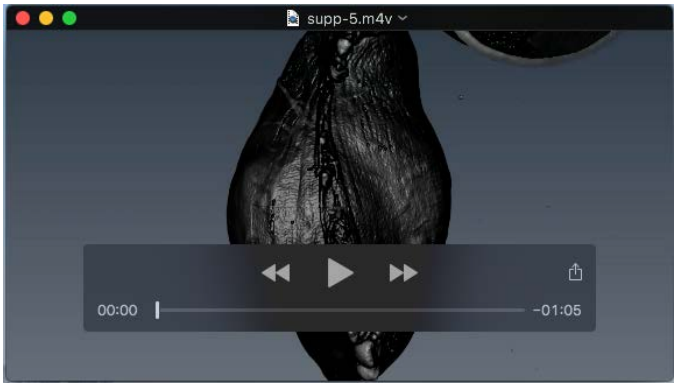

Movie 4: WT1(+) E13.5 embryo imaged *in situ* via micro-CT with Amira segmentation of key volumes. This rendering is also shown in Figure S5A. Note the dorsal volume of the chest cavity in which the lung is growing.

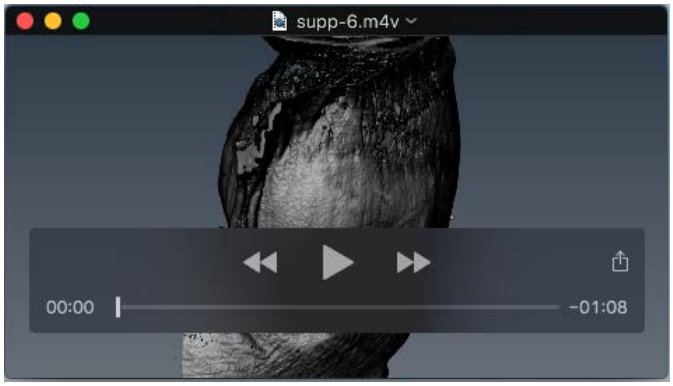

Movie 5: WT1(-) E13.5 embryo imaged *in situ* via micro-CT with Amira segmentation of key volumes. This rendering is also shown in Figure S5B. Note the lack of dorsal volume creating a confined growth environment, and observation of lobe herniation through a bi-lateral diaphragmatic defect into the abdominal cavity.